MATHEMATICAL ENGINEERING TECHNICAL REPORTS

Exact ZF Analysis and Computer-Algebra-Aided Evaluation in Rank-1 LoS Rician Fading

Constantin SIRITEANU, Akimichi TAKEMURA, Christoph KOUTSCHAN, Satoshi KURIKI, Donald St. P. RICHARDS and Hyundong SHIN

METR 2015–24 July 2015

DEPARTMENT OF MATHEMATICAL INFORMATICS
GRADUATE SCHOOL OF INFORMATION SCIENCE AND TECHNOLOGY
THE UNIVERSITY OF TOKYO
BUNKYO-KU, TOKYO 113-8656, JAPAN

WWW page: http://www.keisu.t.u-tokyo.ac.jp/research/techrep/index.html

Exact ZF Analysis and Computer-Algebra-Aided Evaluation in Rank-1 LoS Rician Fading

Constantin Siriteanu, Akimichi Takemura, Christoph Koutschan,
Satoshi Kuriki, Donald St. P. Richards, Hyundong Shin

Abstract

We propose a new exact analysis and evaluation of zero-forcing detection (ZF) for multiple–input/multiple–output (MIMO) spatial multiplexing under transmit-correlated Rician fading for an $N_{\mathrm{R}} \times N_{\mathrm{T}}$ channel matrix with rank-1 line-of-sight (LoS) component. First, an analysis based on several matrix transformations yields the exact signal-to-noise ratio (SNR) moment generating function (m.g.f.) as an infinite series of gamma distribution m.g.f.'s. This produces analogous series for the SNR probability density function and for ZF performance measures. However, their numerical convergence is inherently problematic with increasing Rician K-factor, N_{R}, and N_{T}. Therefore, we additionally derive corresponding differential equations by using computer algebra. Finally, we apply the holonomic gradient method (HGM), i.e., we solve the differential equations by starting from suitable initial conditions computed with the infinite series. HGM yields more reliable performance evaluation than by infinite series alone and more expeditious than by simulation, for realistic values of K, and even for N_{R} and N_{T} relevant to large MIMO systems. We anticipate that future MIMO analyses for Rician fading will produce even more involved series that may benefit from the proposed computer-algebra-aided evaluation approach.

Index Terms

Computer algebra, creative telescoping, differential equation, Gröbner basis, holonomic function, holonomic gradient method, large MIMO, Rayleigh and Rician (Ricean) fading, zero-forcing detection.

C. Siriteanu is with the Graduate School of Information Science and Technology, Osaka University, Japan.

A. Takemura is with the Graduate School of Information Science and Technology, University of Tokyo, Japan.

C. Koutschan is with the Johann Radon Inst. for Comput. and Applied Math., Austrian Academy of Sciences, Linz, Austria.

S. Kuriki is with the Institute of Statistical Mathematics, Tachikawa, Tokyo, Japan.

D. St. P. Richards is with the Department of Statistics, Pennsylvania State University, University Park, PA, USA.

H. Shin is with the Department of Electronics and Radio Engineering, Kyung Hee University, South Korea.

I. INTRODUCTION

A. Background, Motivation, and Scope

The performance of multiple–input/multiple–output (MIMO) wireless communications systems has remained under research focus as the multiantenna architectures that attempt to harvest MIMO gains have continued to evolve, e.g., from single-user MIMO, to multi-user and distributed MIMO, and, most recently, to massive or large MIMO [1] – [7].

As the numbers of transmitting and receiving antennas, herein denoted with N_T and N_R, respectively, have increased in seeking higher array, diversity, and multiplexing gains [1, pp. 72, 64, 385], transceiver processing complexity has also increased. Then, for spatial multiplexing transmission, linear detection methods [3] [5] [6], e.g., zero-forcing detection (ZF) and minimum mean-squared-error detection (MMSE), are feasible because of their relatively-low complexity order $\mathcal{O}(N_\mathrm{R}N_\mathrm{T} + N_\mathrm{R}N_\mathrm{T}^2 + N_\mathrm{T}^3)$ [6], and effective because of their near-optimum performance for $N_\mathrm{R} \gg N_\mathrm{T}$, as the columns of the $N_\mathrm{R} \times N_\mathrm{T}$ channel matrix $\mathbf{H}$ tend to become independent [6].

For increased practical relevance, MIMO channel model complexity has also been increasing, and, with it, the difficulties of MIMO performance analysis and numerical evaluation. Thus, conventionally, MIMO research assumed zero-mean, i.e., Rayleigh fading, for the elements of $\mathbf{H}$, which enabled relatively simple analysis and evaluation [8] [9] [10]. Recently, various cases of nonzero-mean $\mathbf{H}$, i.e., Rician fading, have rendered difficult the performance analysis and evaluation for several transceiver methods [11] – [21]. Rician fading can occur due to line-of-sight (LoS) propagation, in indoor, urban, and suburban scenarios, as shown by the WINNER II project measurements [22, Section 2.3].

WINNER II [22, Table 5.5] has also characterized as lognormal the distributions of 1) the Rician K-factor, which determines the strength of the channel mean vs. standard deviation [1, p. 37], and 2) the azimuth spread (AS), which determines the antenna correlation [23, p. 136]. An ability to evaluate MIMO performance over the entire range of realistic values of K and AS is useful, e.g., in averaging over their distributions, which has rarely been attempted [24].

Thus, we focus herein on evaluating MIMO spatial multiplexing with ZF under Rician fading that is transmit-correlated. For tractable analysis, as in [15] [16], we assume that the LoS or deterministic component of $\mathbf{H}$ satisfies $\mathrm{rank}(\mathbf{H}_\mathrm{d}) = r = 1$. Whereas for LoS propagation r can take any value from 1 to N_T [25], small antenna apertures, relatively-low carrier frequency, or large transmitter-receiver distance, as in point-to-point deployments [1] [16], are likely to yield $\mathbf{H}_\mathrm{d}$ as outer product of array response vectors [1, Eq. (7.29), p. 299], which implies $r = 1$.

Our future work shall consider $r > 1$, MMSE, and more general fading [26] and deployments [17]. Higher r improves $\mathbf{H}$ conditioning, i.e., MIMO performance, and is becoming increasingly more relevant due to envisioned LoS millimeter-wave applications [25] and distributed antennas [17]. Further, MMSE is appealing because it outperforms ZF. Finally, more general fading and deployment types shall enable more realistic performance predictions for future MIMO systems.

B. Limitations of Relevant Previous Work on MIMO ZF

Historically, the study of MIMO ZF commenced with that for uncorrelated Rayleigh fading from [8]. The case of transmit-correlated Rayleigh fading was elucidated in [9] [10]. For Rician fading, previous studies have assumed certain values for r and/or proceeded by approximation:

- Rician fading only for the intended stream, i.e., *Rician–Rayleigh fading*, which is a special case with $r = 1$, or the interfering streams (i.e., Rayleigh–Rician fading, with $r = N_\mathrm{T} - 1$) as may occur in heterogeneous networks. Then, we derived in [18] exact infinite-series expressions for performance measures, e.g., the average error probability, outage probability, and ergodic capacity (i.e., rate [15] [17]) — see more about this previous work below.
- Rician fading for all streams, i.e., *full-Rician* fading, with $r = 1$. Then, solely results from bounds and approximations are available. For example, for uncorrelated fading, [15, Eqs. (55)–(58)] show tight bounds for the sum rate. Other studies approximated the noncentral-Wishart distribution of $\mathbf{H}^\mathcal{H}\mathbf{H}$ with a central-Wishart distribution of equal mean — see [24] and references therein. However, we have shown in [21] [24] that $r = 1$ does not necessarily make this approximation reliable. Thus, only very careful usage in [24] helped average the performance over WINNER II distributions of K and AS.
- Rician fading, $\forall r = 1, \cdots, N_\mathrm{T}$. For this most general case, exact sum-rate expressions for $N_\mathrm{R} \to \infty$ and approximations for finite N_R were derived in [17].

Let us explain our recent exact ZF performance analyses and evaluations for Rician–Rayleigh fading from [18] [19] [20]. In [18], we expressed the moment generating function (m.g.f.) of the signal-to-noise ratio (SNR) in terms of the confluent hypergeometric function ${}_1F_1(\cdot,\cdot,\sigma)$ [18, Eq. (31)], where $\sigma \propto K N_\mathrm{R} N_\mathrm{T}$. Thereafter, its well-known expansion around $\sigma_0 = 0$

[18, Eq. (30)] yielded an infinite series of gamma distribution m.g.f.'s [18, Eq. (37)]. Finally, inverse-Laplace transformation and integration yielded analogous series for the SNR probability density function (p.d.f.), average error probability, outage probability, and ergodic capacity [18, Eqs. (39), (58), (69), (71)]. However, the Wishart distribution noncentrality induced by Rician fading has led to numerical divergence with increasing K, N_R, and N_T for these series' truncation as in [18, Section V.F] [19, Section IV.A], although they theoretically converge everywhere [19].

This problem was tackled in [20] by using the fact that ${}_1F_1(\cdot,\cdot,\sigma)$ is a *holonomic function*[1], i.e., it satisfies a differential equation [20, Eq. (27)] with polynomial coefficients with respect to (w.r.t.) σ. Starting from it, a difficult by-hand derivation produced differential equations for the SNR m.g.f. and then for the p.d.f., via inverse-Laplace transform. Thereafter, we computed reliably the p.d.f. at realistic values of K — but only for relatively small N_R and N_T — by numerically solving its differential equations from initial conditions computed with the infinite series for small K. This approach is known as the *holonomic gradient method* (HGM) because, at each step, the function value is updated with the differential gradient [20, Sec. IV.B]. Finally, in [20], the SNR p.d.f. computed with HGM was numerically integrated to evaluate performance measures, i.e., the outage probability and ergodic capacity.

Summarizing, our exact studies for $r = 1$ in [18] [19] [20] are limited by the following:

- Nonfull-Rician (i.e., only Rician–Rayleigh) fading assumption.
- Tedious by-hand derivations of the SNR m.g.f. and p.d.f. differential equations.
- Time-consuming numerical integration of the p.d.f. for performance measure evaluation.
- HGM not tried for large N_R and N_T, e.g., as relevant for large MIMO systems [5] [7].

On the other hand, only approximate analyses exist for full-Rician fading with $r = 1$ [15] [24].

C. Problem Solved in the Current Work; Exact Analysis and Evaluation Approaches

To the best of our knowledge, the performance of MIMO ZF has not yet been studied *exactly* under full-Rician fading even for $r = 1$. Therefore, we pursue this study herein.

First, upon applying a sequence of simplifying matrix transformations, we deduce several theoretical results that help express exactly the m.g.f. of the SNR for any stream as an infinite series[2] with terms in ${}_1F_1(\cdot,\cdot,\cdot)$. Thus, the m.g.f. is rewritten as a double infinite series of

[1] Other examples: rational functions, logarithm, exponential, sine, special functions (orthogonal polynomials, Bessel [27, p. 41]).

[2] This infinite series reduces for Rician–Rayleigh fading to our expression in a single ${}_1F_1(\cdot,\cdot,\cdot)$ in [18, Eq. (31)].

gamma distribution m.g.f.'s, which readily yields analogous series for the SNR p.d.f. and for the performance measures. Finally, they are recast as a generic single infinite series, but its truncation is found to incur numerical divergence with increasing K, N_R, and N_T. Therefore, as in [18], it is necessary to derive corresponding differential equations and apply HGM.

However, because the generic series mentioned above renders intractable a by-hand derivation of corresponding differential equations, we resort to a computer-algebra-aided approach. Thus, we employ the computer-algebra package `HolonomicFunctions` written earlier by one of the authors [27] [28]. It exploits, for holonomic functions, closure properties [20, Section IV.C] [27], the algebraic concept of *Gröbner bases*[3] [30] and *creative telescoping* algorithms [27, Ch. 3] to deduce differential equations for their addition, multiplication, composition, and integration. This computer-algebra-aided approach readily yields differential equations not only for the SNR m.g.f. and p.d.f., but also for the outage probability and ergodic capacity.

Finally, we evaluate ZF performance measures by HGM, i.e., by solving the obtained differential equations starting from initial conditions computed with the infinite series.

D. Contributions

Compared to previous MIMO ZF work by us and others, herein we:

- Tackle full-Rician fading with $r = 1$ in a new exact analysis that reveals that the SNR distribution is an infinite mixture of gamma distributions.
- Circumvent intractable by-hand deductions of indispensable differential equations by using a computer algebra package written earlier by one of the authors.
- Bypass time-consuming numerical integration of the SNR p.d.f. by deducing differential equations for performance measures and applying HGM for their computation.
- Demonstrate that HGM yields accurate performance evaluation for the entire range of realistic values for K, and even for large N_R and N_T, unlike the infinite series alone, and much faster than by simulation.
- Exactly average the ZF performance over WINNER II distributions of K and AS.

[3]Buchberger's algorithm [29] for Gröbner basis computation specializes, for example, to the Euclidean algorithm when applied to univariate polynomials, and to Gaussian elimination when applied to linear polynomials in several variables [30]. Gröbner bases have helped solve communications optimization problems cast as systems of polynomial equations, e.g., for interference alignment [31], coding gain maximization in space–time coding [32]; other relevant applications are listed in [30].

E. Paper Organization

Section II describes our models and assumptions. Section III presents matrix transformations that help express the m.g.f. of the ZF SNR. Section IV derives a generic infinite series for the SNR m.g.f. and p.d.f., as well as for performance measures. Section V discusses the automated derivation of differential equations, which has been accomplished with `HolonomicFunctions` commands as shown in [33]. Finally, Section VI presents numerical results obtained by simulation, series truncation, and HGM. The Appendix shows some proofs and derivation details.

F. Notation

- Scalars, vectors, and matrices are represented with lowercase italics, lowercase boldface, and uppercase boldface, respectively, e.g., y, $\mathbf{h}$, and $\mathbf{H}$; the statement $\mathbf{H} \doteq N_{\mathrm{R}} \times N_{\mathrm{T}}$ indicates N_{R} rows and N_{T} columns for $\mathbf{H}$; the zero vectors and matrices of appropriate dimensions are denoted with $\mathbf{0}$; superscripts $\cdot^{\mathcal{T}}$ and $\cdot^{\mathcal{H}}$ stand for transpose and Hermitian (i.e., complex-conjugate) transpose; $\mathbf{I}_N$ is the $N \times N$ identity matrix.
- $[\cdot]_i$ is the ith element of a vector; $[\cdot]_{i,j}$, $[\cdot]_{i,\bullet}$, and $[\cdot]_{\bullet,j}$ indicate the i,jth element, ith row, and jth column of a matrix; $\|\mathbf{H}\|^2 = \sum_{i=1}^{N_{\mathrm{R}}} \sum_{j=1}^{N_{\mathrm{T}}} |[\mathbf{H}]_{i,j}|^2$ is the squared Frobenius norm.
- $i = 1 : N$ stands for the enumeration $i = 1, 2, \ldots, N$; $\otimes$ stands for the Kronecker product [34, p. 72] ; $\propto$ stands for 'proportional to'; $\Rightarrow$ stands for logical implication; $\overset{(49)}{=}$ means that the ensuing expression follows from Eq. (49).
- $\mathbf{H} \sim \mathcal{CN}\left(\mathbf{H}_{\mathrm{d}}, \mathbf{I}_{N_{\mathrm{R}}} \otimes \mathbf{R}_{\mathrm{T}}\right)$ indicates a complex-valued circularly-symmetric Gaussian random matrix with mean $\mathbf{H}_{\mathrm{d}}$, row covariance $\mathbf{I}_{N_{\mathrm{R}}}$, and column covariance $\mathbf{R}_{\mathrm{T}}$; subscripts $\cdot_{\mathrm{d}}$ and $\cdot_{\mathrm{r}}$ identify, respectively, deterministic and random components; subscript $\cdot_{\mathrm{n}}$ indicates a normalized variable; $\mathbb{E}\{\cdot\}$ denotes statistical average; $Gamma(N, \Gamma_1)$ represents the *gamma* distribution with shape parameter N and scale parameter Γ_1; $\chi_m^2(\delta)$ denotes the noncentral *chi-square* distribution with m degrees of freedom and noncentrality parameter δ; χ_m^2 denotes the central chi-square distribution with m degrees of freedom; $Beta(N, M)$ represents the central *beta* distribution with shape parameters N and M; $Beta(N, M, x)$ represents the noncentral beta distribution with shape parameters N and M, and noncentrality x.
- ${}_1F_1(\cdot;\cdot;\cdot)$ is the *confluent hypergeometric function* [35, Eq. (13.2.2), p. 322]; $(N)_n$ is the Pochhammer symbol, i.e., $(N)_0 = 1$ and $(N)_n = N(N+1)\ldots(N+n-1)$, $\forall n \geq 1$.
- $\partial_t^k g(t,z)$ denotes the kth partial derivative w.r.t. t of function $g(t,z)$.

II. Models and Assumptions

A. Received Signal and Fading Models

We consider an uncoded point-to-point MIMO spatial multiplexing system over a frequency-flat fading channel [1, Chs. 3, 7]. There are $N_{\mathrm{T}} \geq 2$ and $N_{\mathrm{R}} \geq N_{\mathrm{T}}$ antenna elements at the transmitter[4] and receiver, respectively. For the transmit-symbol vector denoted with

$$\mathbf{y} = (y_1 \quad y_2 \quad \cdots \quad y_{N_{\mathrm{T}}})^{\mathcal{T}} \doteq N_{\mathrm{T}} \times 1, \tag{1}$$

the stream of symbols y_i transmitted from antenna i is referred to as Stream i. Without loss of generality, we consider that Stream 1 is the intended stream (i.e., stream whose symbol is detected, and whose detection performance is analyzed and evaluated), and that the remaining

$$N_{\mathrm{I}} = N_{\mathrm{T}} - 1 \tag{2}$$

streams, i.e., Streams $i = 2 : N_{\mathrm{T}}$, are interfering streams. The number of *degrees of freedom* is

$$N = N_{\mathrm{R}} - N_{\mathrm{I}} = N_{\mathrm{R}} - N_{\mathrm{T}} + 1. \tag{3}$$

Then, the vector with the received signals can be represented as

$$\mathbf{r} = \sqrt{\frac{E_{\mathrm{s}}}{N_{\mathrm{T}}}}\mathbf{H}\mathbf{y} + \mathbf{n} \doteq N_{\mathrm{R}} \times 1, \tag{4}$$

where $\frac{E_{\mathrm{s}}}{N_{\mathrm{T}}}$ is the energy transmitted per symbol (i.e., per antenna), and $\mathbf{n} \sim \mathcal{CN}(\mathbf{0}, N_0\,\mathbf{I}_{N_{\mathrm{R}}})$ is the additive noise. Then, the per-symbol transmit-SNR is

$$\Gamma_{\mathrm{s}} = \frac{E_{\mathrm{s}}}{N_0}\frac{1}{N_{\mathrm{T}}}. \tag{5}$$

Finally, we assume that the complex-Gaussian channel matrix $\mathbf{H} \doteq N_{\mathrm{R}} \times N_{\mathrm{T}}$, of rank N_{T}, is perfectly known at the receiver[5]. With its deterministic and random components denoted as $\mathbf{H}_{\mathrm{d}}$ and $\mathbf{H}_{\mathrm{r}}$, respectively, we can write

$$\mathbf{H} = \mathbf{H}_{\mathrm{d}} + \mathbf{H}_{\mathrm{r}} = \sqrt{\frac{K}{K+1}}\mathbf{H}_{\mathrm{d,n}} + \sqrt{\frac{1}{K+1}}\mathbf{H}_{\mathrm{r,n}}, \tag{6}$$

where $\mathbf{H}_{\mathrm{d,n}}$ and $\mathbf{H}_{\mathrm{r,n}}$ are normalized according to [20] [21]

$$\|\mathbf{H}_{\mathrm{d,n}}\|^2 = \mathbb{E}\{\|\mathbf{H}_{\mathrm{r,n}}\|^2\} = N_{\mathrm{R}}N_{\mathrm{T}}, \text{ which implies } \mathbb{E}\{\|\mathbf{H}\|^2\} = N_{\mathrm{R}}N_{\mathrm{T}}, \tag{7}$$

[4]For $N_{\mathrm{T}} = 1$, i.e., maximal-ratio combining, we obtained a simple SNR m.g.f. expression for Rician fading in [18, Eq. (36)].

[5]ZF for imperfectly-known $\mathbf{H}$ can be studied with the effective-SNR approach we described in [24].

and K, known as the Rician K-factor, is described by

$$K = \frac{\|\mathbf{H}_{\rm d}\|^2}{\mathbb{E}\{\|\mathbf{H}_{\rm r}\|^2\}} = \frac{\frac{K}{K+1}\|\mathbf{H}_{\rm d,n}\|^2}{\frac{1}{K+1}\mathbb{E}\{\|\mathbf{H}_{\rm r,n}\|^2\}}. \tag{8}$$

Then, $K = 0$ yields full-Rayleigh fading, i.e., $|\,[\mathbf{H}]_{i,j}\,|$ is Rayleigh distributed $\forall i, j$, as assumed in [8] [9] [10]. Further, the case when $K \neq 0$ and in $\mathbf{H}_{\rm d,n}$ only column $[\mathbf{H}_{\rm d,n}]_{\bullet,1}$ is nonzero is referred to as Rician–Rayleigh fading, as in [18] [19] [20]. Finally, herein, the case when $K \neq 0$ and each column of $\mathbf{H}_{\rm d,n}$ has at least one nonzero element is referred to as full-Rician fading.

We assume that $\mathbf{H}_{\rm d}$ arises due to LoS propagation between transmitter and receiver. Then, if the transmitter–receiver distance is much larger than the antenna interelement spacing, $\mathbf{H}_{\rm d}$ can be represented as the outer product of the array response vectors for the receiving antenna, $\mathbf{a} \doteq N_{\rm R} \times 1$, and transmitting antenna, $\mathbf{b} \doteq N_{\rm T} \times 1$, i.e., [1, Eq. (7.29), p. 299]

$$\mathbf{H}_{\rm d} = \mathbf{a}\mathbf{b}^{\mathcal{H}} = \mathbf{a}\,(b_1^* \quad b_2^* \quad \ldots \quad b_{N_{\rm T}}^*), \tag{9}$$

which reveals that $\mathbf{H}_{\rm d}$ has rank $r = 1$ and columns given by $\mathbf{h}_{{\rm d},i} = \mathbf{a}\,b_i^*, i = 1 : N_{\rm T}$.

Remark 1. *We may assume that* $\|\mathbf{a}\| = 1$ *if we scale* $\mathbf{b}$ *according to*

$$\|\mathbf{b}\|^2 = \sum_{i=1}^{N_T} |b_i|^2 = \sum_{i=1}^{N_T} \underbrace{\|\mathbf{a}\|^2}_{=1} |b_i|^2 = \sum_{i=1}^{N_T} \|\mathbf{h}_{d,i}\|^2 = \|\mathbf{H}_d\|^2 \overset{(6),(7)}{=} \frac{K}{K+1} N_R N_T. \tag{10}$$

For tractable analysis, we assume zero row correlation (i.e., receive-antenna correlation) for $\mathbf{H}$. Also, we assume, as in [9] [10] [18] [19] [20], that any row of $\mathbf{H}_{\rm r,n}$ is distributed as $\mathcal{CN}(\mathbf{0}, \mathbf{R}_{\rm T})$, so that any row of $\mathbf{H}_{\rm r}$ is distributed as $\mathcal{CN}(\mathbf{0}, \mathbf{R}_{{\rm T},K})$ with

$$\mathbf{R}_{{\rm T},K} = \frac{1}{N_{\rm R}}\mathbb{E}\{\mathbf{H}_{\rm r}^{\mathcal{H}}\mathbf{H}_{\rm r}\} = \frac{1}{K+1}\frac{1}{N_{\rm R}}\mathbb{E}\{\mathbf{H}_{\rm r,n}^{\mathcal{H}}\mathbf{H}_{\rm r,n}\} = \frac{1}{K+1}\mathbf{R}_{\rm T}, \tag{11}$$

so that $\mathbf{H} \sim \mathcal{CN}\left(\mathbf{H}_{\rm d}, \mathbf{I}_{N_{\rm R}} \otimes \mathbf{R}_{{\rm T},K}\right)$.

Matrix $\mathbf{R}_{\rm T}$ is determined by antenna interelement spacing and AS, i.e., the 'standard deviation' of the power azimuth spectrum [23, p. 136]. When the latter is modeled as Laplacian, as recommended by WINNER II [22], $\mathbf{R}_{\rm T}$ can be computed from the AS with [23, Eqs. (4-3)–(4-5)].

Remark 2. *WINNER II modeled the measured AS (in degrees) and* K *(in dB) as random variables with scenario-dependent lognormal distributions [22, Table 5.5] [24, Table 1]. Thus, herein, we attempt to evaluate ZF performance for AS and* K *values relevant to these distributions.*

B. Matrix Partitioning Used in Analysis

To study Stream-1 detection performance[6] we shall employ the partitioning

$$\mathbf{H} = (\mathbf{h}_1 \quad \mathbf{H}_2) = (\mathbf{h}_{\mathrm{d},1} \quad \mathbf{H}_{\mathrm{d},2}) + (\mathbf{h}_{\mathrm{r},1} \quad \mathbf{H}_{\mathrm{r},2}), \tag{12}$$

where $\mathbf{h}_1$, $\mathbf{h}_{\mathrm{d},1}$, and $\mathbf{h}_{\mathrm{r},1}$ are $N_{\mathrm{R}} \times 1$ vectors, whereas $\mathbf{H}_2$, $\mathbf{H}_{\mathrm{d},2}$, and $\mathbf{H}_{\mathrm{r},2}$ are $N_{\mathrm{R}} \times N_{\mathrm{I}}$ matrices. We shall also employ the corresponding partitioning of the column covariance matrix, i.e.,

$$\mathbf{R}_{\mathrm{T},K} = \begin{pmatrix} \mathbf{R}_{\mathrm{T},K_{11}} & \mathbf{R}_{\mathrm{T},K_{12}} \\ \mathbf{R}_{\mathrm{T},K_{21}} & \mathbf{R}_{\mathrm{T},K_{22}} \end{pmatrix} = \begin{pmatrix} r_{\mathrm{T},K_{11}} & \mathbf{r}^{\mathcal{H}}_{\mathrm{T},K_{21}} \\ \mathbf{r}_{\mathrm{T},K_{21}} & \mathbf{R}_{\mathrm{T},K_{22}} \end{pmatrix}. \tag{13}$$

Remark 3. *Herein, we consider full-Rician fading with $r = rank(\mathbf{H}_d) = rank(\mathbf{H}_{d,2}) = 1$, whereas in [18] [20] we considered its special case of Rician–Rayleigh fading, i.e., $rank(\mathbf{H}_d) = 1$, but $rank(\mathbf{H}_{d,2}) = 0$. Thus, the results obtained herein specialize to those in [18] [20] when we reduce to $\mathbf{0}$ the vector formed with the last $N_I = N_T - 1$ elements of $\mathbf{b}$, i.e., the vector*

$$\widetilde{\mathbf{b}} = (b_2 \quad \dots \quad b_{N_T})^{\mathcal{T}}. \tag{14}$$

III. Exact Analysis of ZF

A. ZF SNR as Hermitian Form

Given $\mathbf{H}$, ZF for the signal from (4) refers to symbol detection based on the operation

$$\sqrt{\frac{N_{\mathrm{T}}}{E_{\mathrm{s}}}} \left[\mathbf{H}^{\mathcal{H}}\mathbf{H}\right]^{-1} \mathbf{H}^{\mathcal{H}}\, \mathbf{r} = \mathbf{y} + \frac{1}{\sqrt{\Gamma_{\mathrm{s}}}} \left[\mathbf{H}^{\mathcal{H}}\mathbf{H}\right]^{-1} \mathbf{H}^{\mathcal{H}} \frac{\mathbf{n}}{\sqrt{N_0}}. \tag{15}$$

Based on (15) and [10] [18], the SNR for Stream 1 can be written as the Hermitian form below:

$$\gamma_1 = \frac{\Gamma_{\mathrm{s}}}{\left[(\mathbf{H}^{\mathcal{H}}\mathbf{H})^{-1}\right]_{1,1}} = \Gamma_{\mathrm{s}} \mathbf{h}_1^{\mathcal{H}} \left[\mathbf{I}_{N_{\mathrm{R}}} - \mathbf{H}_2 (\mathbf{H}_2^{\mathcal{H}} \mathbf{H}_2)^{-1} \mathbf{H}_2^{\mathcal{H}}\right] \mathbf{h}_1 = \Gamma_{\mathrm{s}} \mathbf{h}_1^{\mathcal{H}} \mathbf{Q}_2 \mathbf{h}_1. \tag{16}$$

Remark 4. *The following transformations do not change the ZF SNR in (16):*

- *Row transformations of $\mathbf{H}$ with unitary matrices, because they do not change $\mathbf{H}^{\mathcal{H}}\mathbf{H}$.*
- *Column transformations of $\mathbf{H}_2$ with nonsingular matrices, because they do not change $\mathbf{Q}_2$.*

Several such transformations shown below help simplify the SNR distribution analysis.

[6]Without loss of generality, because of the full-Rician model adopted in (9).

B. Row Transformation $\mathbf{F} = \mathbf{V}\mathbf{H}$ *That Zeroes Rows* $[\mathbf{F}_d]_{i,\bullet}$, $i = 2 : N_R$

If we make the substitution $\mathbf{H} = \mathbf{V}^{\mathcal{H}}\mathbf{F}$, with unitary $\mathbf{V} \doteq N_{\mathrm{R}} \times N_{\mathrm{R}}$, in (16) and partition according to (12) the matrix

$$\mathbf{F} = \mathbf{V}\mathbf{H} = (\mathbf{f}_1 \quad \mathbf{F}_2) = (\mathbf{f}_{\mathrm{d},1} \quad \mathbf{F}_{\mathrm{d},2}) + (\mathbf{f}_{\mathrm{r},1} \quad \mathbf{F}_{\mathrm{r},2}) \doteq N_{\mathrm{R}} \times N_{\mathrm{T}}, \tag{17}$$

the SNR expression (16) becomes

$$\gamma_1 = \Gamma_{\mathrm{s}} \mathbf{f}_1^{\mathcal{H}} \mathbf{Q}_2 \mathbf{f}_1, \tag{18}$$

and the idempotent and rank-N matrix $\mathbf{Q}_2 \doteq N_{\mathrm{R}} \times N_{\mathrm{R}}$ can be written as

$$\mathbf{Q}_2 = \mathbf{I}_{N_{\mathrm{R}}} - \mathbf{H}_2(\mathbf{H}_2^{\mathcal{H}}\mathbf{H}_2)^{-1}\mathbf{H}_2^{\mathcal{H}} = \mathbf{I}_{N_{\mathrm{R}}} - \mathbf{F}_2(\mathbf{F}_2^{\mathcal{H}}\mathbf{F}_2)^{-1}\mathbf{F}_2^{\mathcal{H}}. \tag{19}$$

Choosing the first row of the unitary matrix $\mathbf{V}$ as $[\mathbf{V}]_{1,\bullet} = \mathbf{a}^{\mathcal{H}}$, we conveniently obtain

$$[\mathbf{F}_{\mathrm{d}}]_{1,\bullet} \overset{(9)}{=} ([\mathbf{V}]_{1,\bullet}\,\mathbf{a})\mathbf{b}^{\mathcal{H}} = \|\mathbf{a}\|^2\mathbf{b}^{\mathcal{H}} = \mathbf{b}^{\mathcal{H}}, \quad \text{(Row 1)} \tag{20}$$

$$[\mathbf{F}_{\mathrm{d}}]_{i,\bullet} \overset{(9)}{=} \underbrace{([\mathbf{V}]_{i,\bullet}\,\mathbf{a})}_{=0}\mathbf{b}^{\mathcal{H}} = \mathbf{0}, \;\; i = 2 : N_{\mathrm{R}}, \quad (\text{Rows } 2 : N_{\mathrm{R}}) \tag{21}$$

$$\Rightarrow [\mathbf{F}_{\mathrm{d}}]_{\bullet,j} = \mathbf{f}_{\mathrm{d},j} = \begin{pmatrix} b_j^* & 0 & \dots & 0 \end{pmatrix}^{\mathcal{T}}, \; j = 1 : N_{\mathrm{T}}, \text{ (All columns)}. \tag{22}$$

Theorem 1. *The m.g.f. of the SNR conditioned on* $\mathbf{Q}_2$ *can be written, simply, as*

$$M_{\gamma_1|\mathbf{Q}_2}(s) = \mathbb{E}_{\gamma_1}\{e^{s\gamma_1}|\mathbf{Q}_2\} = \frac{1}{(1-\Gamma_1 s)^N}\exp\left\{f_1(s)[\mathbf{Q}_2]_{1,1}\right\}, \tag{23}$$

where scalar Γ_1 *and function* $f_1(s)$ *are defined in the proof below.*

Proof: Because the column covariance of $\mathbf{F} = \mathbf{V}\mathbf{H}$ is the same as that of $\mathbf{H}$, i.e., $\mathbf{R}_{\mathrm{T},K}$, partitioned as in (13), and because $\mathbf{f}_1 \doteq N_{\mathrm{R}} \times 1$ and $\mathbf{F}_2 \doteq N_{\mathrm{R}} \times N_{\mathrm{I}}$ from the partitioning of $\mathbf{F}$ in (17) are jointly Gaussian, the distribution of $\mathbf{f}_1$ given $\mathbf{F}_2$ is given by [10, Appendix] [18, Eqs. (12)-(16)]

$$\mathbf{f}_1|\mathbf{F}_2 \sim \mathcal{CN}\left(\underbrace{(\mathbf{f}_{\mathrm{d},1} - \mathbf{F}_{\mathrm{d},2}\mathbf{r}_{2,1})}_{=\boldsymbol{\mu}\doteq N_{\mathrm{R}}\times 1} + \mathbf{F}_2\mathbf{r}_{2,1}, \left(\left[\mathbf{R}_{\mathrm{T},K}^{-1}\right]_{1,1}\right)^{-1}\mathbf{I}_{N_{\mathrm{R}}}\right), \text{with} \tag{24}$$

$$\mathbf{r}_{2,1} = \mathbf{R}_{\mathrm{T},K_{22}}^{-1}\mathbf{r}_{\mathrm{T},K_{21}} \doteq N_{\mathrm{I}} \times 1, \tag{25}$$

$$\left(\left[\mathbf{R}_{\mathrm{T},K}^{-1}\right]_{1,1}\right)^{-1} = r_{\mathrm{T},K_{11}} - \mathbf{r}_{\mathrm{T},K_{21}}^{\mathcal{H}}\mathbf{R}_{\mathrm{T},K_{22}}^{-1}\mathbf{r}_{\mathrm{T},K_{21}} \doteq 1 \times 1. \tag{26}$$

Then, it can be shown by substituting (24) into (18) and further manipulating as in [10] [18], that the SNR conditioned on $\mathbf{Q}_2$ from (18) can be written as the Hermitian form

$$\begin{aligned}
\gamma_1|\mathbf{Q}_2 &= \Gamma_1 \widetilde{\mathbf{f}}_1^{\mathcal{H}} \mathbf{Q}_2 \widetilde{\mathbf{f}}_1, \quad \text{with} && (27)\\
\Gamma_1 &= \frac{\Gamma_{\text{s}}}{\left[\mathbf{R}_{\text{T},K}^{-1}\right]_{1,1}}, && (28)\\
\widetilde{\mathbf{f}}_1 &\sim \mathcal{CN}\left(\sqrt{\left[\mathbf{R}_{\text{T},K}^{-1}\right]_{1,1}}\boldsymbol{\mu}, \mathbf{I}_{N_{\text{R}}}\right), && (29)\\
\boldsymbol{\mu} &\overset{(24)}{=} \mathbf{f}_{\text{d},1} - \mathbf{F}_{\text{d},2}\mathbf{r}_{2,1} \overset{(22)}{=} (b_1^* - \widetilde{\mathbf{b}}^{\mathcal{H}}\mathbf{r}_{2,1} \quad 0 \quad \ldots \quad 0)^{\mathcal{T}} = (\mu_1 \quad 0 \quad \ldots \quad 0)^{\mathcal{T}}. && (30)
\end{aligned}$$

Thus, transformation (17) yielded a single nonzero-mean element in $\widetilde{\mathbf{f}}_1$, simplifying analysis.

The Hermitian form in $\widetilde{\mathbf{f}}_1$ from (27) helps cast the m.g.f. of the SNR given $\mathbf{Q}_2$ as [18, Eq. (20)]

$$\begin{aligned}
M_{\gamma_1|\mathbf{Q}_2}(s) &= \frac{\exp\left\{-x_1\boldsymbol{\nu}^{\mathcal{H}}\left[\mathbf{I}_{N_{\text{R}}} - (\mathbf{I}_{N_{\text{R}}} - \Gamma_1 s\mathbf{Q}_2)^{-1}\right]\boldsymbol{\nu}\right\}}{\det\left(\mathbf{I}_{N_{\text{R}}} - \Gamma_1 s \mathbf{Q}_2\right)}, \quad \text{with} && (31)\\
x_1 &= \left[\mathbf{R}_{\text{T},K}^{-1}\right]_{1,1}\|\boldsymbol{\mu}\|^2 = \left[\mathbf{R}_{\text{T},K}^{-1}\right]_{1,1}|\mu_1|^2, && (32)\\
\boldsymbol{\nu} &= \frac{\boldsymbol{\mu}}{\mu_1} = (1 \quad 0 \quad \ldots \quad 0)^{\mathcal{T}}, && (33)\\
\mathbf{I}_{N_{\text{R}}} - (\mathbf{I}_{N_{\text{R}}} - \Gamma_1 s\mathbf{Q}_2)^{-1} &= -\frac{\Gamma_1 s}{1-\Gamma_1 s}\mathbf{Q}_2. && (34)
\end{aligned}$$

Above, (34) follows by using the eigendecomposition of $\mathbf{Q}_2$. The desired m.g.f. expression in (23) ensues by substituting (34) and (33) into (31) and defining $f_1(s) = \frac{\Gamma_1 s}{1-\Gamma_1 s} x_1$. ■

C. Partial Column Transformations That Help Rewrite $[\mathbf{Q}_2]_{1,1}$ Conveniently

1) Unitary Transformation $\mathbf{E}_2 = \mathbf{F}_2\widetilde{\mathbf{V}}$ That Zeroes Elements $[\mathbf{E}_{d,2}]_{1,j}$, $j = 2 : N_I$: Making the substitution $\mathbf{F}_2 = \mathbf{E}_2\widetilde{\mathbf{V}}^{\mathcal{H}}$, with unitary $\widetilde{\mathbf{V}} \doteq N_{\text{I}} \times N_{\text{I}}$, in (19) yields

$$\mathbf{Q}_2 = \mathbf{I}_{N_{\text{R}}} - \mathbf{F}_2(\mathbf{F}_2^{\mathcal{H}}\mathbf{F}_2)^{-1}\mathbf{F}_2^{\mathcal{H}} = \mathbf{I}_{N_{\text{R}}} - \mathbf{E}_2(\mathbf{E}_2^{\mathcal{H}}\mathbf{E}_2)^{-1}\mathbf{E}_2^{\mathcal{H}}. \quad (35)$$

Based on (17), we can write

$$\mathbf{E}_2 = \mathbf{F}_2\widetilde{\mathbf{V}} = \mathbf{F}_{\text{d},2}\widetilde{\mathbf{V}} + \mathbf{F}_{\text{r},2}\widetilde{\mathbf{V}} = \mathbf{E}_{\text{d},2} + \mathbf{E}_{\text{r},2} \doteq N_{\text{R}} \times N_{\text{I}}. \quad (36)$$

Setting $[\widetilde{\mathbf{V}}]_{\bullet,1} = \widetilde{\mathbf{b}}/\|\widetilde{\mathbf{b}}\|$ simplifies the ensuing SNR analysis as it zeroes $[\mathbf{E}_{\text{d},2}]_{1,j}$, $j = 2 : N_{\text{I}}$:

$$\mathbf{E}_{\text{d},2} = \mathbf{F}_{\text{d},2}\widetilde{\mathbf{V}} \overset{(22)}{=} \begin{pmatrix} \widetilde{\mathbf{b}}^{\mathcal{H}} \\ \mathbf{0} \end{pmatrix} \begin{pmatrix} \frac{\widetilde{\mathbf{b}}}{\|\widetilde{\mathbf{b}}\|} & [\widetilde{\mathbf{V}}]_{\bullet,2} \cdots [\widetilde{\mathbf{V}}]_{\bullet,N_{\text{I}}} \end{pmatrix} = \|\widetilde{\mathbf{b}}\| \begin{pmatrix} 1 & \mathbf{0} \\ \mathbf{0} & \mathbf{0} \end{pmatrix}. \quad (37)$$

2) Nonsingular Transformation That Decorrelates the Columns of $\mathbf{E}_2$*:* For the column correlation of $\mathbf{E}_{\mathrm{r},2}$ from (36), i.e., for

$$\frac{1}{N_{\mathrm{R}}}\mathbb{E}\{\mathbf{E}_{\mathrm{r},2}^{\mathcal{H}}\mathbf{E}_{\mathrm{r},2}\} = \frac{1}{N_{\mathrm{R}}}\mathbb{E}\{(\mathbf{F}_{\mathrm{r},2}\widetilde{\mathbf{V}})^{\mathcal{H}}(\mathbf{F}_{\mathrm{r},2}\widetilde{\mathbf{V}})\} = \frac{1}{N_{\mathrm{R}}}\widetilde{\mathbf{V}}^{\mathcal{H}}\mathbb{E}\{\mathbf{F}_{\mathrm{r},2}^{\mathcal{H}}\mathbf{F}_{\mathrm{r},2}\}\widetilde{\mathbf{V}} \overset{(13)}{=} \widetilde{\mathbf{V}}^{\mathcal{H}}\mathbf{R}_{\mathrm{T},K_{22}}\widetilde{\mathbf{V}}, \quad (38)$$

let us consider the Cholesky decomposition [34, Sec. 5.6]

$$\widetilde{\mathbf{V}}^{\mathcal{H}}\mathbf{R}_{\mathrm{T},K_{22}}\widetilde{\mathbf{V}} = \mathbf{A}\mathbf{A}^{\mathcal{H}}, \quad (39)$$

where $\mathbf{A} \doteq N_{\mathrm{I}} \times N_{\mathrm{I}}$ is upper triangular with real-valued and positive diagonal elements.

Then, considering a matrix with uncorrelated elements distributed as $[\mathbf{E}_{\mathrm{w},2}]_{i,j} \sim \mathcal{CN}(0,1)$, $i = 1 : N_{\mathrm{R}}, j = 1 : N_{\mathrm{I}}$, we can write (36) based on (39) and (38) as

$$\mathbf{E}_2 = \mathbf{E}_{\mathrm{d},2} + \mathbf{E}_{\mathrm{w},2}\mathbf{A}^{\mathcal{H}} = \left(\mathbf{E}_{\mathrm{d},2}\mathbf{A}^{-\mathcal{H}} + \mathbf{E}_{\mathrm{w},2}\right)\mathbf{A}^{\mathcal{H}}, \quad (40)$$

Thus, by transforming the columns of $\mathbf{E}_2$ with $\mathbf{A}^{-\mathcal{H}}$, we obtain

$$\mathbf{G}_2 = \mathbf{E}_2\mathbf{A}^{-\mathcal{H}} = \mathbf{E}_{\mathrm{d},2}\mathbf{A}^{-\mathcal{H}} + \mathbf{E}_{\mathrm{w},2} \doteq N_{\mathrm{R}} \times N_{\mathrm{I}}, \quad (41)$$

whose mean that can be written, based on (37) and the fact that $\mathbf{A}^{-\mathcal{H}}$ is lower triangular, as

$$\mathbf{G}_{\mathrm{d},2} = \mathbf{E}_{\mathrm{d},2}\mathbf{A}^{-\mathcal{H}} = \|\widetilde{\mathbf{b}}\|[\mathbf{A}^{-\mathcal{H}}]_{1,1}\begin{pmatrix} 1 & \mathbf{0} \\ \mathbf{0} & \mathbf{0} \end{pmatrix}. \quad (42)$$

Furthermore, the derivation from Appendix A yields

$$x_2 = \|\mathbf{G}_{\mathrm{d},2}\|^2 \overset{(42)}{=} \|\widetilde{\mathbf{b}}\|^2([\mathbf{A}^{-\mathcal{H}}]_{1,1})^2 \overset{(79)}{=} \widetilde{\mathbf{b}}^{\mathcal{H}}\mathbf{R}_{\mathrm{T},K_{22}}^{-1}\widetilde{\mathbf{b}}. \quad (43)$$

Remark 5. *For Rician–Rayleigh fading, Remark 3 revealed that* $\widetilde{\mathbf{b}} = \mathbf{0}$*, which by (43) implies* $x_2 = 0$*. On the other hand, for full-Rayleigh fading, (32) implies that also* $x_1 = 0$*.*

Thus, column transformation (41) yielded $\mathbf{G}_2$ with uncorrelated columns and mean given by

$$[\mathbf{G}_{\mathrm{d},2}]_{i,j} = \begin{cases} \sqrt{x_2} & \text{, (i.e., real-valued) for } i = j = 1, \\ 0 & \text{, otherwise.} \end{cases} \quad (44)$$

Upon substituting $\mathbf{E}_2 = \mathbf{G}_2\mathbf{A}^{\mathcal{H}}$ in (35), i.e.,

$$\mathbf{Q}_2 = \mathbf{I}_{N_{\mathrm{R}}} - \mathbf{G}_2\mathbf{A}^{\mathcal{H}}(\mathbf{A}\mathbf{G}_2^{\mathcal{H}}\mathbf{G}_2\mathbf{A}^{\mathcal{H}})^{-1}\mathbf{A}\mathbf{G}_2^{\mathcal{H}} = \mathbf{I}_{N_{\mathrm{R}}} - \mathbf{G}_2(\mathbf{G}_2^{\mathcal{H}}\mathbf{G}_2)^{-1}\mathbf{G}_2^{\mathcal{H}}, \quad (45)$$

the tractability of our SNR distribution analysis benefits from the simple statistics of $\mathbf{G}_2$ (vs. $\mathbf{F}_2$), as shown below.

3) QR Decomposition: Finally, by substituting in (45) the QR decomposition [34, Sec. 5.7]

$$\mathbf{G}_2 = \mathbf{U}_2\mathbf{T}_2, \tag{46}$$

where $\mathbf{U}_2 \doteq N_\mathrm{R} \times N_\mathrm{I}$ satisfies $\mathbf{U}_2^\mathcal{H}\mathbf{U}_2 = \mathbf{I}_{N_\mathrm{I}}$, and $\mathbf{T}_2 \doteq N_\mathrm{I} \times N_\mathrm{I}$ is upper triangular with real-valued and positive diagonal elements, we can write $\mathbf{Q}_2$ simply as

$$\mathbf{Q}_2 = \mathbf{I}_{N_\mathrm{R}} - \mathbf{U}_2\mathbf{T}_2(\mathbf{T}_2^\mathcal{H}\mathbf{T}_2)^{-1}\mathbf{T}_2^\mathcal{H}\mathbf{U}_2^\mathcal{H} = \mathbf{I}_{N_\mathrm{R}} - \mathbf{U}_2\mathbf{U}_2^\mathcal{H}. \tag{47}$$

This helps write $[\mathbf{Q}_2]_{1,1}$ for the m.g.f. in (23) solely in terms of the first row of $\mathbf{U}_2$ as

$$\begin{aligned}[\mathbf{Q}_2]_{1,1} &= 1 - [\mathbf{U}_2]_{1,\bullet}\left([\mathbf{U}_2]_{1,\bullet}\right)^\mathcal{H} = 1 - \left(|[\mathbf{U}_2]_{1,1}|^2 + |[\mathbf{U}_2]_{1,2}|^2 + \cdots + |[\mathbf{U}_2]_{1,N_\mathrm{I}}|^2\right) \\ &= \underbrace{(1 - |[\mathbf{U}_2]_{1,1}|^2)}_{=\beta_1}\underbrace{\left(1 - \frac{|[\mathbf{U}_2]_{1,2}|^2 + \cdots + |[\mathbf{U}_2]_{1,N_\mathrm{I}}|^2}{1 - |[\mathbf{U}_2]_{1,1}|^2}\right)}_{=\beta_2}.\end{aligned} \tag{48}$$

D. The Main Analysis Result: Exact M.G.F. Expression of the Unconditioned SNR

The above transformations have helped write the conditioned-SNR m.g.f. from (23) as

$$M_{\gamma_1}(s \mid \beta_1, \beta_2) = \frac{1}{(1 - \Gamma_1 s)^N}\exp\{f_1(s)\beta_1\beta_2\}. \tag{49}$$

In order to express the unconditioned-SNR m.g.f., we need to average (49) over the distributions of β_1 and β_2, which are elucidated in the following two lemmas.

Lemma 1. *Random variable β_1 from (48) is distributed as*

$$\beta_1 \sim Beta(N_R - 1, 1, x_2). \tag{50}$$

Proof: See Appendix B. ■

Lemma 2. *Random variable β_2 from (48) is distributed as*

$$\beta_2 \sim Beta(N, N_I - 1), \tag{51}$$

i.e., with m.g.f. [18, Eq. (30)]

$$M_{\beta_2}(s) = {}_1F_1(N; N_R - 1; s), \tag{52}$$

and is independent of β_1.

Proof: See Appendix C. ■

Theorem 2. *The m.g.f. of the unconditioned SNR for ZF under full-Rician fading with $r = 1$ is*

$$M_{\gamma_1}(s; x_1, x_2) = \frac{e^{-x_2}}{(1-\Gamma_1 s)^N} \sum_{n_2=0}^{\infty} \frac{x_2^{n_2}}{n_2!} {}_1F_1\left(N; n_2 + N_R; \frac{\Gamma_1 s}{1-\Gamma_1 s} x_1\right). \tag{53}$$

Proof: See Appendix D. ■

The above reduces for Rician–Rayleigh fading (i.e., for $x_2 = 0$) to [18, Eqs. (31), (37)]

$$\begin{aligned} M_{\gamma_1}(s; x_1) &= \frac{1}{(1-\Gamma_1 s)^N} {}_1F_1\left(N; N_{\mathrm{R}}; \frac{\Gamma_1 s}{1-\Gamma_1 s} x_1\right), & (54)\\ &= \sum_{n_1=0}^{\infty} \frac{(N)_{n_1}}{(N_{\mathrm{R}})_{n_1}} \frac{x_1^{n_1}}{n_1!} \sum_{m_1=0}^{n_1} \binom{n_1}{m_1} (-1)^{m_1} \underbrace{\frac{1}{(1-s\Gamma_1)^{N+n_1-m_1}}}_{=M_{n_1,m_1}(s)}, & (55)\end{aligned}$$

where (55) follows from (54) by the infinite-series expansion around $\sigma_0 = 0$ [18, Eq. (30)]

$${}_1F_1(N; N_{\mathrm{R}}; \sigma) = \sum_{n=0}^{\infty} \frac{(N)_n}{(N_{\mathrm{R}})_n} \frac{\sigma^n}{n!}. \tag{56}$$

Theoretically, (56) converges $\forall \sigma$ [19, Section III.B]. Nevertheless, inherent numerical convergence difficulties with increasing σ [36] have encumbered the computation of ensuing measures, e.g., the ZF SNR p.d.f. for Rician–Rayleigh fading at realistic values of K [18] [19] [20].

IV. Exact Infinite Series Expressions for Performance Measures

A. Exact Double Infinite Series for M.G.F., P.D.F., and Performance Measures

By substituting (56) into (53) and proceeding as for (55), the SNR m.g.f. becomes

$$M_{\gamma_1}(s; x_1, x_2) = e^{-x_2} \sum_{n_1=0}^{\infty} \sum_{n_2=0}^{\infty} \frac{(N)_{n_1}}{(n_2 + N_{\mathrm{R}})_{n_1}} \frac{x_1^{n_1}}{n_1!} \frac{x_2^{n_2}}{n_2!} \underbrace{\sum_{m_1=0}^{n_1} \binom{n_1}{m_1} (-1)^{m_1} M_{n_1,m_1}(s)}_{=M_{n_1}(s)}. \tag{57}$$

Using the m.g.f.–p.d.f. Laplace-transform pair corresponding to $Gamma(N + n_1 - m, \Gamma_1)$, i.e.,

$$M_{n_1,m_1}(s) = \frac{1}{(1-s\Gamma_1)^{N+n_1-m_1}} \overset{Laplace}{\longleftrightarrow} \frac{t^{(N+n_1-m_1)-1} e^{-t/\Gamma_1}}{[(N+n_1-m_1)-1]!\, \Gamma_1^{N+n_1-m_1}} = p_{n_1,m_1}(t), \tag{58}$$

the ZF SNR p.d.f. corresponding to (57) can be written, analogously, as:

$$p_{\gamma_1}(t; x_1, x_2) = e^{-x_2} \sum_{n_1=0}^{\infty} \sum_{n_2=0}^{\infty} \frac{(N)_{n_1}}{(n_2 + N_{\mathrm{R}})_{n_1}} \frac{x_1^{n_1}}{n_1!} \frac{x_2^{n_2}}{n_2!} \underbrace{\sum_{m_1=0}^{n_1} \binom{n_1}{m_1} (-1)^{m_1} p_{n_1,m_1}(t)}_{=p_{n_1}(t)}. \tag{59}$$

By integrating (59), the Stream-1 outage probability at threshold SNR τ and the ergodic capacity (i.e., rate) are exactly characterized by analogous infinite series, i.e.,

$$P_{\mathrm{o}}(x_1,x_2) = \int_0^{\tau} p_{\gamma_1}(t;x_1,x_2)\,\mathrm{d}t \tag{60}$$

$$= e^{-x_2}\sum_{n_1=0}^{\infty}\sum_{n_2=0}^{\infty}\frac{(N)_{n_1}}{(n_2+N_{\mathrm{R}})_{n_1}}\frac{x_1^{n_1}}{n_1!}\frac{x_2^{n_2}}{n_2!}\underbrace{\sum_{m_1=0}^{n_1}\binom{n_1}{m_1}(-1)^{m_1}P_{\mathrm{o},n_1,m_1}}_{=P_{\mathrm{o},n_1}}, \tag{61}$$

$$C(x_1,x_2) = \frac{1}{\ln 2}\int_0^{\infty}\ln(1+t)p_{\gamma_1}(t;x_1,x_2)\,\mathrm{d}t \tag{62}$$

$$= e^{-x_2}\sum_{n_1=0}^{\infty}\sum_{n_2=0}^{\infty}\frac{(N)_{n_1}}{(n_2+N_{\mathrm{R}})_{n_1}}\frac{x_1^{n_1}}{n_1!}\frac{x_2^{n_2}}{n_2!}\underbrace{\sum_{m_1=0}^{n_1}\binom{n_1}{m_1}(-1)^{m_1}C_{n_1,m_1}}_{=C_{n_1}}, \tag{63}$$

where, from (58), we have[7]

$$P_{\mathrm{o},n_1,m_1} = \int_0^{\tau} p_{n_1,m_1}(t)\,\mathrm{d}t = \frac{\gamma\left(N+n_1-m_1,\tau/\Gamma_1\right)}{[(N+n_1-m_1)-1]!}, \tag{64}$$

$$C_{n_1,m_1} = \frac{1}{\ln 2}\int_0^{\infty}\ln(1+t)\frac{t^{(N+n_1-m_1)-1}e^{-t/\Gamma_1}}{[(N+n_1-m_1)-1]!\,\Gamma_1^{N+n_1-m_1}}\,\mathrm{d}t. \tag{65}$$

Finally, by following the approach in [18, Section V.A], the average error probability can also be expressed as an infinite series analogous to (61) and (63).

B. Generic Infinite Series for M.G.F., P.D.F., and Performance Measures

The analogous series (57), (59), (61), (63) can be written as the generic double infinite series

$$h(x_1,x_2) = e^{-x_2}\sum_{n_1=0}^{\infty}\sum_{n_2=0}^{\infty}\frac{(N)_{n_1}}{(N_{\mathrm{R}}+n_2)_{n_1}}H_{n_1}\frac{x_1^{n_1}}{n_1!}\frac{x_2^{n_2}}{n_2!}, \tag{66}$$

where H_{n_1} stands for $M_{n_1}(s)$ from (57), $p_{n_1}(t)$ from (59), P_{o,n_1} from (61), and C_{n_1} from (63). Numerical results not shown due to length limitations have revealed that increasing K, N_{R}, and N_{T} yield increasingly problematic numerical convergence for series (66). This is explained by 1) the fact that (57) has been obtained from (53) by replacing ${}_1F_1\left(N;n_2+N_{\mathrm{R}};\frac{\Gamma_1 s}{1-\Gamma_1 s}x_1\right)$ with its expansion around $x_1=0$ from (56); and 2) the fact that x_1 is increasing because of the following proportionality, proved in Appendix E:

$$x_1 \propto K N_{\mathrm{R}} N_{\mathrm{T}}. \tag{67}$$

[7] $\gamma(k,x)=\int_0^x t^{k-1}e^{-t}\,\mathrm{d}t$ is the *incomplete gamma function* [35, p. 174]. Integral (65) is expressed in [18, Eq. (73)].

Appendix E also shows that $x_2 \propto K N_\mathrm{R} N_\mathrm{T}$. In fact, the expressions for x_1 and x_2 deduced in (103) and (104) can be used to show that their ratio $c_1 = \frac{x_1}{x_2}$ is real-valued, positive, and independent of K and N_R. Finally, numerical results have revealed that $c_1 < 1$ and $c_1 \propto 1/N_\mathrm{T}$. This justifies making the substitutions $x_2 = z$ and $x_1 = c_1 z$ to improve numerical behavior.

Lemma 3. *For $x_2 = z$ and $x_1 = c_1 z$, series (66) can be recast as the single infinite series*

$$h(z) = e^{-z} \sum_{n=0}^{\infty} G_n \frac{z^n}{n!}, \quad \textit{where } G_n(z) = \sum_{m=0}^{n} \binom{n}{m} \frac{(N)_m}{(N_R + n - m)_m} H_m c_1^m. \tag{68}$$

The derivatives of $h(z)$, required below for HGM, are given by

$$\partial_z^k h(z) = \sum_{l=0}^{k} \binom{k}{l} (-1)^{k-l} e^{-z} \sum_{n=l}^{\infty} G_n \frac{z^{n-l}}{(n-l)!}. \tag{69}$$

Proof: The proof of the first part is not shown, due to simplicity and length limitations. The second part follows from (68) based on Leibniz's formula [35, Eq. (1.4.12), p. 5]. ■

However, numerical results shown later reveal that the truncation of (68) still does not converge reliably for practically relevant values of K, N_R, and N_T. Therefore, we endeavor to compute it by HGM, as done for Rician–Rayleigh fading in [20] to compute the SNR p.d.f. series deduced from (55). Recall that HGM evaluates a function at given values for its variables by numerically solving its differential equations starting from initial conditions, i.e., known values of the function and required derivatives, at another point [20, Sec. IV.B]. Thus, HGM requires differential equations.

By-hand derivations based on (54) and the differential equation for ${}_1F_1(N; N_\mathrm{R}; \sigma)$ [20, Eq. (27)]

$$\sigma \cdot {}_1F_1^{(2)}(N; N_\mathrm{R}; \sigma) + (N_\mathrm{R} - \sigma) \cdot {}_1F_1^{(1)}(N; N_\mathrm{R}; \sigma) - N \cdot {}_1F_1(N; N_\mathrm{R}; \sigma) = 0, \tag{70}$$

yielded, with difficulty, the differential equations for the ZF SNR m.g.f. and p.d.f. for Rician–Rayleigh fading in [20, Eqs. (32), (42)]. As (68) is more complicated than (54), by-hand derivation from (68) is intractable. Instead, we employ the automated approach described next to derive differential equations for $h(z)$ — i.e., for $M_{\gamma_1}(s; z)$, $p_{\gamma_1}(t; z)$, $P_\mathrm{o}(z)$, and $C(z)$.

V. Computer-Algebra-Aided Derivation of Differential Equations for HGM

A. Holonomic Functions, Annihilator, Gröbner Basis, and Creative Telescoping

A function is *holonomic* w.r.t. a set of continuous variables if it satisfies for each of them a linear differential equation with polynomial coefficients. A function is holonomic w.r.t. to a set of discrete variables if the associated generating function is holonomic in the previous sense [20, Sec. IV.C] [27, p. 17]. For example, ${}_1F_1(N; N_{\mathrm{R}}; \sigma)$ is holonomic w.r.t. σ because it satisfies differential equation[8] (70). In other words, ${}_1F_1(N; N_{\mathrm{R}}; \sigma)$ is *annihilated* by the differential operator $\sigma\partial_\sigma^2 + (N_{\mathrm{R}} - \sigma)\partial_\sigma - N$. The (infinite) set of all operators that annihilate a given holonomic function is called its *annihilator* [27, p. 18].

Holonomic functions are closed under addition, multiplication, certain substitutions, and taking sums and integrals [20] [27]. Consequently, functions $M_{\gamma_1}(s; z)$, $p_{\gamma_1}(t; z)$, $P_{\mathrm{o}}(z)$, and $C(z)$, cast as in (68), are holonomic. The fact that the closure properties for holonomic functions can be executed algorithmically provides a systematic way of deriving the differential equations required for HGM, by starting with the annihilating operators of the comprised "elementary" holonomic functions in (68). A key ingredient for algorithmically executing closure properties is the algebraic concept of *Gröbner basis*, which provides a canonical and finite representation of an annihilator and helps decide whether an operator is in an annihilator. For details on *Gröbner bases* theory, computation, and applications see [29] [27] [31] [32] [30] and references therein.

While many holonomic closure properties require, basically, only linear algebra, computing the annihilator for a sum or integral of a holonomic function is a more involved task. For example, one can employ the *creative telescoping* technique: given an integral $F(x) = \int_a^b f(x, y)\,\mathrm{d}y$, creative telescoping algorithmically finds in the annihilator of $f(x, y)$ a differential operator of the form $P(x, \partial_x) + \partial_y \cdot Q(x, y, \partial_x, \partial_y)$. Then, using the fundamental theorem of calculus [35, p. 6] and differentiating under the integral sign reveals[9] $P(x, \partial_x)$ as an annihilating operator for $F(x)$ [27, p. 46]. Several creative telescoping algorithms are described in [27, Ch. 3].

B. The `HolonomicFunctions` Computer-Algebra Package

This freely-available computer-algebra package written earlier in `Mathematica` by one of the authors, is described, with numerous examples, in [28]. Its commands implement: 1) the computation of Gröbner bases in operator algebras, 2) closure properties for holonomic functions, and 3) creative telescoping algorithms from [27, Ch. 3]. Thus, it enables automated deduction of differential equations for holonomic functions (e.g., our m.g.f. infinite series), their Laplace

[8]Note that ${}_1F_1(N; N_{\mathrm{R}}; \sigma)$ is also holonomic w.r.t. N and N_{R}.

[9]Under "natural boundary" conditions [27].

transform (e.g., our p.d.f.), and their integrals (e.g., our outage probability and ergodic capacity). Conveniently, its symbolic-computation ability[10] allows for parameters (e.g., N_{R}, N, Γ_1, τ, c_1).

C. Computer-Algebra-Aided Derivation Procedure and Results

The `Mathematica` file with `HolonomicFunctions` commands that produce the output presented below can be downloaded from [33]. Therein, for example, Gröbner basis computation with the command `Annihilator` yields annihilating operators for expression $e^{-z}\frac{z^n}{n!}$ from (68). Further, the command `CreativeTelescoping` yields annihilating operators for G_n based on the summation in (68), and for $P_{\mathrm{o}}(z)$ based on the integral in (60).

Note that the particular functions that enter the differential equations shown below — i.e., $M_{\gamma_1}(s;z)$, $\partial_s M_{\gamma_1}(s;z)$, $\partial_z M_{\gamma_1}(s;z)$; $p_{\gamma_1}(t;z)$, $\partial_t p_{\gamma_1}(t;z)$, $\partial_z p_{\gamma_1}(t;z)$, $\partial_z^2 p_{\gamma_1}(t;z)$; $\partial_z^k P_{\mathrm{o}}(z)$, $k = 0:4$; $\partial_z^k C(z)$, $k = 0:6$ — arise automatically from (68) by Gröbner basis computation and creative telescoping, and are revealed with the command `UnderTheStaircase` in [33].

The steps and outcomes of the procedure implemented by the code in [33] are as follows:

1) Derive SNR m.g.f. differential equations w.r.t. s and z, based on (68). Then, [33] reveals that the function vector

$$\mathbf{m}(s;z) = (M_{\gamma_1}(s;z) \quad \partial_s M_{\gamma_1}(s;z) \quad \partial_z M_{\gamma_1}(s;z))^{\mathcal{T}} \doteq 3 \times 1 \tag{71}$$

satisfies the systems of differential equations w.r.t. s and z

$$\partial_s \mathbf{m}(s;z) = \mathbf{\Theta}_s \mathbf{m}(s;z), \quad \partial_z \mathbf{m}(s;z) = \mathbf{\Theta}_z \mathbf{m}(s;z), \tag{72}$$

with the 3×3 matrices $\mathbf{\Theta}_s$ and $\mathbf{\Theta}_z$ shown only in [33], due to space limitations.

2) Using results from Step 1, derive p.d.f. differential equations w.r.t. t and z, based on the inverse-Laplace transform. Then, [33] reveals that the function vector

$$\mathbf{p}(t;z) = (p_{\gamma_1}(t;z) \quad \partial_t p_{\gamma_1}(t;z) \quad \partial_z p_{\gamma_1}(t;z) \quad \partial_z^2 p_{\gamma_1}(t;z))^{\mathcal{T}} \doteq 4 \times 1 \tag{73}$$

satisfies the systems of differential equations w.r.t. t and z

$$\partial_t \mathbf{p}(t;z) = \Xi_t \mathbf{p}(t;z), \quad \partial_z \mathbf{p}(t;z) = \Xi_z \mathbf{p}(t;z), \tag{74}$$

with the 4×4 matrices Ξ_t and Ξ_z shown only in [33], due to space limitations.

[10] Inherited from `Mathematica`.

TABLE I

THE ELEMENTS OF COMPANION MATRIX $\mathbf{\Phi}_z \doteq 5 \times 5$ FROM THE SYSTEM OF DIFFERENTIAL EQUATIONS (75).

Element	Expression
$[\mathbf{\Phi}_z]_{i,i+1},\ i = 1:4$	1
$[\mathbf{\Phi}_z]_{5,2}$	$\frac{1}{\Gamma_1 z^3}\big(-c_1\tau N_{\rm R} + 2\Gamma_1 N_{\rm R} + c_1\Gamma_1 N_{\rm R} + c_1\Gamma_1 N N_{\rm R} + c_1\tau N_{\rm R}^2 - 2\Gamma_1 N_{\rm R}^2 - c_1\Gamma_1 N_{\rm R}^2$ $- c_1\Gamma_1 N N_{\rm R}^2 + c_1\tau N_{\rm R} z - 4\Gamma_1 N_{\rm R} z - 5c_1\Gamma_1 N_{\rm R} z - c_1^2\Gamma_1 N_{\rm R} z - c_1\Gamma_1 N N_{\rm R} z$ $- c_1^2\Gamma_1 N N_{\rm R} z - 2\Gamma_1 z^2 - 4c_1\Gamma_1 z^2 - 2c_1^2\Gamma_1 z^2\big)$
$[\mathbf{\Phi}_z]_{5,3}$	$\frac{1}{\Gamma_1 z^3}\big(\Gamma_1 N_{\rm R} - \Gamma_1 {N_{\rm R}}^3 + 2c_1\tau N_{\rm R} z - 7\Gamma_1 N_{\rm R} z - 4c_1\Gamma_1 N_{\rm R} z - 2c_1\Gamma_1 N N_{\rm R} z$ $- 3\Gamma_1 N_{\rm R}^2 z - 2c_1\Gamma_1 N_{\rm R}^2 z + c_1\tau z^2 - 7\Gamma_1 z^2 - 9c_1\Gamma_1 z^2 - 2c_1^2\Gamma_1 z^2 - c_1\Gamma_1 N z^2$ $- c_1^2\Gamma_1 N z^2 - 3\Gamma_1 N_{\rm R} z^2 - 4c_1\Gamma_1 N_{\rm R} z^2 - c_1^2\Gamma_1 N_{\rm R} z^2 - \Gamma_1 z^3 - 2c_1\Gamma_1 z^3 - c_1^2\Gamma_1 z^3\big)$
$[\mathbf{\Phi}_z]_{5,4}$	$\frac{1}{\Gamma_1 z^2}\big(-3\Gamma_1 N_{\rm R} - 3\Gamma_1 N_{\rm R}^2 + c_1\tau z - 8\Gamma_1 z - 5c_1\Gamma_1 z - c_1\Gamma_1 N z - 6\Gamma_1 N_{\rm R} z$ $- 4c_1\Gamma_1 N_{\rm R} z - 3\Gamma_1 z^2 - 4c_1\Gamma_1 z^2 - c_1^2\Gamma_1 z^2\big)$
$[\mathbf{\Phi}_z]_{5,5}$	$\frac{1}{z}\big(-3 - 3N_{\rm R} - 3z - 2c_1 z\big)$
Other	0

3) Using results from Step 2, derive differential equations w.r.t. z for $P_{\rm o}(z)$ and $C(z)$, based on their integral relationships from (60) and (62) with $p_{\gamma_1}(t;z)$. Then, [33] reveals that the function vector $\mathbf{p}_{\rm o}(z) \doteq 5 \times 1$ with $[\mathbf{p}_{\rm o}(z)]_k = \partial_z^{k-1} P_{\rm o}(z)$, $k = 0:4$, and $\mathbf{c}(z) \doteq 7 \times 1$ with $[\mathbf{c}(z)]_k = \partial_z^{k-1} C(z)$, $k = 0:6$, satisfy the systems of differential equations

$$\partial_z \mathbf{p}_{\rm o}(z) = \mathbf{\Phi}_z \mathbf{p}_{\rm o}(z), \tag{75}$$

$$\partial_z \mathbf{c}(z) = \mathbf{\Psi}_z \mathbf{c}(z), \tag{76}$$

where $\mathbf{\Phi}_z \doteq 5 \times 5$ and $\mathbf{\Psi}_z \doteq 7 \times 7$ are companion matrices [34, p. 109]; the former is depicted in Table I, whereas the latter is shown only in [33], due to space limitations.

The systems of differential equations deduced above enable the HGM-based computation of the SNR p.d.f., outage probability, and ergodic capacity. HGM results for the computation of the outage probability are shown below.

VI. Numerical Results

A. Description of Parameter Settings and Approaches

For the channel-matrix mean model in (9), unit-norm vector $\mathbf{a}$ and vector $\mathbf{b}$ with the norm in (10) are constructed, according to [1, Eq. (7.29), p. 299], from array response vectors[11] as

$$\mathbf{a} = \frac{1}{\sqrt{N_{\mathrm{R}}}}(1 \quad e^{-j\pi\cos(\theta_{\mathrm{R}})} \quad \dots \quad e^{-j\pi(N_{\mathrm{R}}-1)\cos(\theta_{\mathrm{R}})})^{\mathcal{T}}, \tag{77}$$

$$\mathbf{b} = \frac{1}{\sqrt{N_{\mathrm{T}}}}(1 \quad e^{-j\pi\cos(\theta_{\mathrm{T}})} \quad \dots \quad e^{-j\pi(N_{\mathrm{T}}-1)\cos(\theta_{\mathrm{T}})})^{\mathcal{T}}\sqrt{\frac{K}{K+1}N_{\mathrm{R}}N_{\mathrm{T}}}, \tag{78}$$

assuming uniform linear antenna arrays with interelement spacing of half of the carrier wavelength. Above, θ_{R} and θ_{T} are, respectively, the angles of arrival and departure of the LoS component w.r.t. the antenna broadside directions. We show results for θ_{T} equal to the central angle, θ_{c}, of the transmit-side Laplacian power azimuth spectrum[12] [23, Eq. (4.2)]. Then, we have computed $\mathbf{R}_{\mathrm{T}}$ from the AS with [23, Eqs. (4-3)–(4-5)].

Due to limited space, we can show results only for the Stream-1 outage probability[13] for $\tau = 8.2$ dB, which corresponds to a symbol error probability of 10^{-2} for QPSK modulation. Then, the constellation size is $M = 4$, and we show P_{o} vs. $\Gamma_{\mathrm{b}} = \Gamma_{\mathrm{s}}/\log_2 M = \Gamma_{\mathrm{s}}/2$. The ergodic capacity can be computed similarly, using (68), (69), and (76) with $\mathbf{\Psi}_z$ deduced in [33].

Unless stated otherwise, presented results have been obtained by running `MATLAB R2012a`, in its native fixed precision, on a computer with a 3.4-GHz, 64-bit, quad-core[14] processor and 8 GB of memory. For the simulation results (in figure legends: `Sim.`) we have employed, when feasible, $N_{\mathrm{s}} = 10^6$ samples of $\mathbf{n}$ and $\mathbf{H}$ for (4), to produce reliable results for P_{o} as low as 10^{-5}. Then, series results (in legends: `Series`) have been produced by truncating (68) as in [18, Section V.F] [19, Section IV.A], i.e., new terms have been added until: 1) their relative change falls below 10^{-10} [19, Eq. (34)], or 2) $n \leq n_{\max} = 150$ (additional terms in (68) lead to numerical divergence because the arising large numbers are represented with poor precision — for further details see also [19, Section IV.B]). Numerical divergence is indicated in legends with `Series`*. Full-Rayleigh fading results (in legend: `Rayleigh,Exp.`) have been obtained with expression

[11] See [1, Fig. 7.3b, p. 296, Eq. (7.20), p. 297] for geometry and derivation details.

[12] Unshown results have revealed that $\theta_{\mathrm{c}} = \theta_{\mathrm{T}}$ is the worst-case scenario, i.e., ZF performance improves with larger $|\theta_{\mathrm{c}} - \theta_{\mathrm{T}}|$.

[13] The outage probability can be evaluated analogously for any other stream.

[14] Nevertheless, we have run single instances of `MATLAB` when measuring the computation time (with `tic`, `toc`.)

$P_{\mathrm{o}} = \frac{\gamma(N,\tau/\Gamma_1)}{(N-1)!}$, obtained from (61) based on Remark 5. Finally, HGM results (in legends: `HGM`) have been produced by solving — with the `MATLAB ode45` function with tolerance levels of 10^{-10} — the system of differential equations (75). The initial condition $\mathbf{p}_{\mathrm{o}}(z_0)$ has been computed with (69) for $z_0 = 0.05692$ obtained with (43) for $K = -25$ dB, $N_{\mathrm{R}} = 6$, $N_{\mathrm{T}} = 4$, and $\mathbf{R}_{\mathrm{T}} = \mathbf{I}_{N_{\mathrm{T}}}$. This choice enables the accurate computation of $\partial_z^k P_{\mathrm{o}}(z_0)$ with series (69).

Finally, results are shown for K and AS values relevant to their lognormal distributions for WINNER II scenarios A1 (indoors office) and C2 (urban macrocell), under LoS propagation [22, Table 5.5]: 1) averages of these distributions, i.e., for $K = 7$ dB, and for AS $= 51°$ and $11°$, which yield low and high antenna element correlation, i.e., $|[\mathbf{R}_{\mathrm{T}}]_{1,2}| = 0.12$ and 0.83, respectively; 2) values within the range of most likely values [24, Table 1], or 3) random samples[15].

B. Description of Results for K and AS Relevant to Scenario A1, and for Small N_R and N_T

Fig. 1 shows results for AS $= 51°$ and K set to values from 0 dB to the upper limit of the range expected with 0.99 probability for scenario A1 [24, Table 1]. Note that the `MATLAB` series truncation diverges for $K = 14$ dB and 21 dB[16], whereas HGM and simulation results agree at all K. Thus, HGM enables us to investigate the performance degradation likely to occur in practice with increasing K for MIMO ZF under full-Rician fading with $r = 1$.

Fig. 2 shows results from averaging also over AS and K from their WINNER II lognormal distributions for scenario A1. First, simulation has not been attempted due to the long required time. (The computation time is explored in more detail below.) Series truncation does not yield useful results because of numerical divergence for the larger K values. Only HGM has yielded relatively expeditiously a smooth plot whose unshown continuation at sufficiently large Γ_{b} has revealed the expected diversity order[17] of $N = N_{\mathrm{R}} - N_{\mathrm{T}} + 1 = 3$ [18, Eq. (46)].

Figs. 1 and 2 depict the same Γ_{b} range in order to reveal that 1) setting AS and K to their means can substantially overestimate the performance compared to averaging over AS and K — compare the blue dash-dotted plot in Fig. 1 with the solid black plot in Fig. 2; and 2) making the

[15]Then, even just computing $\mathbf{R}_{\mathrm{T}}$ with [23, Eqs. (4-3)–(4-5)] is time consuming; nevertheless, the employed $2,100$ samples of AS and K have yielded smooth outage probability plots.

[16]Our series truncation in `Mathematica`, with its arbitrary precision, converged also for $K = 14$ dB, but required an hour instead of a few seconds for the HGM. Thus, series truncation in `Mathematica` was not tried for $K = 21$ dB.

[17]The expected diversity order is also noticeable from the plots for $K = 0$ dB and 7 dB in Fig. 1.

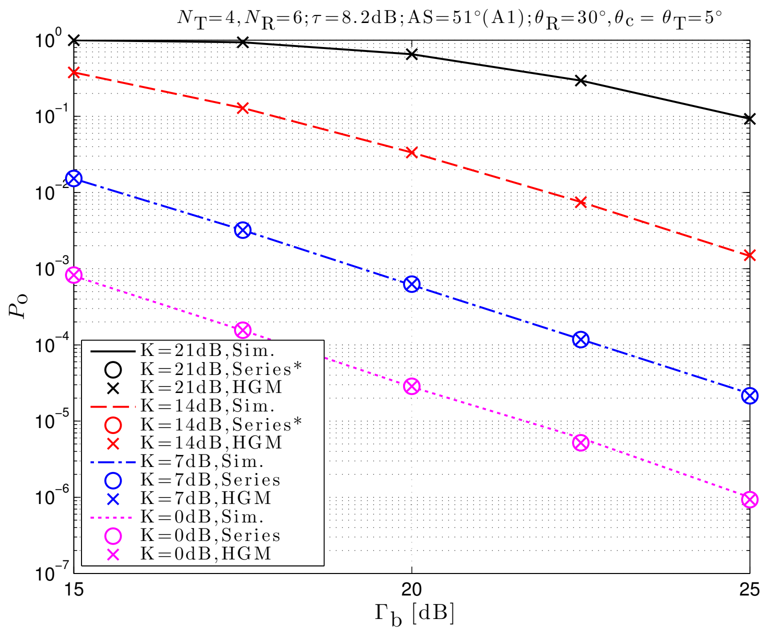

Fig. 1. Stream-1 outage probability for $N_R = 6$, $N_T = 4$, AS $= 51°$ (i.e., scenario A1 mean), and various values of K, including $K = 7$ dB (i.e., scenario A1 mean). Series results for $K = 14, 21$ dB do not appear because of numerical divergence.

assumption of full-Rayleigh fading instead of full-Rician fading leads to unrealistic performance expectations — compare the plots in Fig. 2.

C. Description of Results for K, AS Relevant to Scenarios A1, C2, and for Increasing N_R, N_T

Table II summarizes compactly results of several numerical experiments for K and AS set to their averages for scenarios A1 and C2, and for the pair (N_R, N_T) set to $N_a \times (6, 4)$, with N_a shown in the second column[18]. The Γ_b ranges shown in the third column yield P_o in the order of 10^{-2} – 10^{-5}, as shown in the fourth column. The remaining three columns show the actual or estimated computation time (in seconds), per Γ_b value. The marks ✓ and ✗ in the 'Series' column denote, respectively, successful and unsuccessful (i.e., numerical divergence) series computation[19]. Further, mark ✗ in the 'Sim.' column indicates infeasible simulation duration. Finally, mark ✓ in the 'HGM' column indicates successful HGM-based computation.

[18]Note that N_R does not necessarily have to be much larger than N_T even in massive MIMO [7].

[19]For $(N_R = 6, N_T = 4)$ numerical convergence is achieved with $n = 134$, whereas the other (N_R, N_T) pairs yield $n = n_{\max} = 150$. Consequently, MATLAB reports about the same computation time (≈ 1.3 s) for all cases.

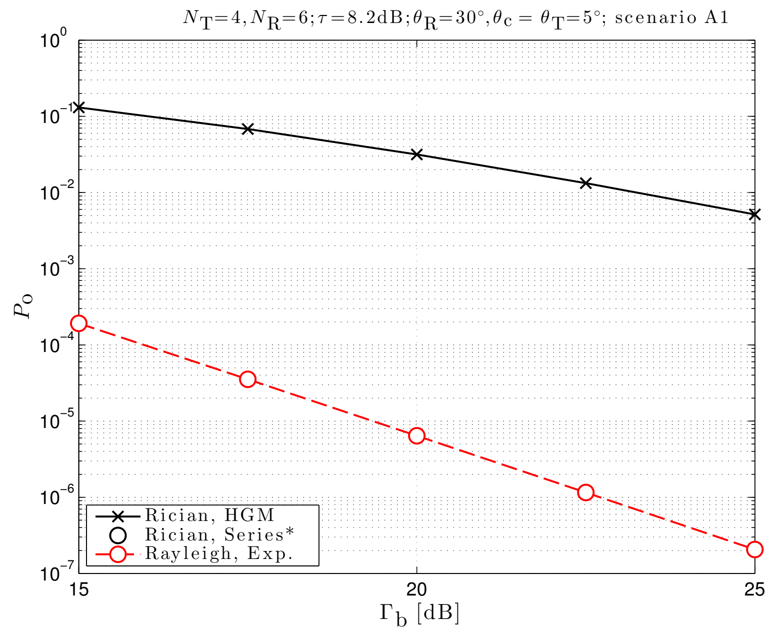

Fig. 2. Stream-1 outage probability for $N_R = 6$, $N_T = 4$, averaged also over the WINNER II lognormal distributions of K and AS for scenario A1. Results corresponding to `Rician, Series` do not appear because of numerical divergence.

Fig. 3 characterizes ZF performance for $K = 7$ dB and AS $= 51°$, and for the large-MIMO setting with $N_R = 100$ and $N_T = 20$. On the one hand, series truncation does not produce useful results; on the other hand, HGM results agree with the simulation results, and we have found HGM over 30 times faster[20]. Thus, unlike series truncation and simulation, HGM enables reliable, accurate, and expeditious ZF assessments even for large MIMO.

VII. Summary, Conclusions, and Future Work

Summarizing, this paper has provided an exact performance analysis and evaluation of MIMO spatial multiplexing with ZF, under transmit-correlated full-Rician fading with LoS component of rank $r = 1$. First, we expressed as infinite series the SNR m.g.f. and p.d.f., as well as performance measures, e.g., the outage probability and ergodic capacity. However, their numerical convergence has been revealed inherently more problematic with increasing K, N_R, and

[20]When large N_T yields infeasibly-long simulation, HGM results can be validated by checking the diversity order revealed by its P_o-vs.-Γ_b plot. E.g., for $N_R = 104$ and $N_T = 100$, we have found its slope magnitude to be near the expected $N = 5$.

TABLE II

RESULTS FOR $K = 7$ DB, AS $= 51°$ (I.E., SCENARIO A1) AND AS $= 11°$ (C2), AND $(N_R, N_T) = N_a \times (6,4)$.

AS	N_a	Γ_b (dB)	$P_o = [a \times 10^{-2}, b \times 10^{-5}]$	Series	Sim. ($N_s = 10^6$)	HGM
51° (A1)	1	[15, 25]	$a = 1.53, b = 2.15$	1.3 s ✓	31 s	20 s ✓
51° (A1)	2	[11, 17]	$a = 1.74, b = 4.26$	1.3 s ✗	53 s	20 s ✓
51° (A1)	5	[6, 9]	$a = 1.39, b = 6.39$	1.3 s ✗	520 s	20 s ✓
51° (A1)	10	[2, 4.5]	$a = 2.35, b = 2.45$	1.3 s ✗	2,300 s	20 s ✓
51° (A1)	15	[0, 2]	$a = 1.98, b = 1.61$	1.3 s ✗	8,800 s	20 s ✓
51° (A1)	100	[-9.2, -8.5]	$a = 2.72, b = 2.57$	1.3 s ✗	$estimated: 1.9 \times 10^6$ s ✗	20 s ✓
11° (C2)	1	[23, 32]	$a = 1.12, b = 3.01$	1.3 s ✓	31 s	20 s ✓
11° (C2)	2	[18.5, 24.5]	$a = 1.43, b = 3.36$	1.3 s ✗	54 s	20 s ✓
11° (C2)	10	[5, 7.5]	$a = 2.12, b = 2.09$	1.3 s ✗	2,400 s	20 s ✓

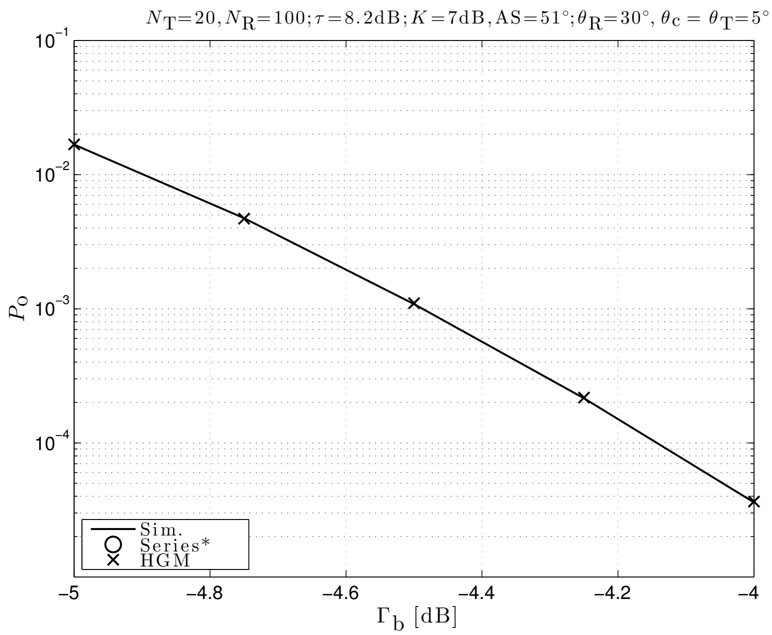

Fig. 3. Stream-1 outage probability for $N_R = 100$, $N_T = 20$, for $K = 7$ dB and AS $= 51°$ (i.e., averages for scenario A1). Results corresponding to `Series` do not appear because of numerical divergence.

N_T. Therefore, we have applied computer algebra to the derived infinite series and deduced corresponding differential equations. They have been used for HGM-based computation. Thus, we have expeditiously produced accurate results for the range of realistic values of K and even for large N_R and N_T. Consequently, we have been able to assess the substantial performance degradation incurred with increasing K for ZF when $r = 1$. Furthermore, HGM has helped reveal that the performance averaged over WINNER II AS and K distributions can be much worse than that for average AS and K. Finally, we have been able to evaluate the performance for antenna numbers relevant to large MIMO reliably and much more expeditiously than by simulation. In future work, we shall consider cases with higher r, more general fading and deployment models, and other transceiver processing methods. We expect that such cases will yield exact expressions as multiple infinite series for MIMO performance measures. Then, we shall employ computer algebra to deduce the corresponding differential equations before HGM-based computation.

APPENDIX

A. Derivation of $([\mathbf{A}^{-\mathcal{H}}]_{1,1})^2$ for Eq. (43)

Using (39), the fact that $\mathbf{A}^{-1}$ is upper triangular and $\mathbf{A}^{-\mathcal{H}} = (\mathbf{A}^{-1})^{\mathcal{H}}$ is lower triangular, and the fact that $[\mathbf{A}^{-1}]_{i,i}$, $\forall i = 1 : N_{\text{I}}$, are real-valued yields, respectively,

$$(\mathbf{A}\mathbf{A}^{\mathcal{H}})^{-1} = \mathbf{A}^{-\mathcal{H}}\mathbf{A}^{-1} = \widetilde{\mathbf{V}}^{\mathcal{H}}\mathbf{R}_{\text{T},K_{22}}^{-1}\widetilde{\mathbf{V}},\ [(\mathbf{A}\mathbf{A}^{\mathcal{H}})^{-1}]_{1,1} = [\mathbf{A}^{-\mathcal{H}}]_{1,1}[\mathbf{A}^{-1}]_{1,1},\ [\mathbf{A}^{-\mathcal{H}}]_{1,1} = [\mathbf{A}^{-1}]_{1,1}.$$

Then, also recalling the choice $[\widetilde{\mathbf{V}}]_{\bullet,1} = \widetilde{\mathbf{b}}/\|\widetilde{\mathbf{b}}\|$ made to obtain (37), we can write:

$$\begin{aligned}([\mathbf{A}^{-\mathcal{H}}]_{1,1})^2 &= [\mathbf{A}^{-\mathcal{H}}]_{1,1}[\mathbf{A}^{-1}]_{1,1} = [(\mathbf{A}\mathbf{A}^{\mathcal{H}})^{-1}]_{1,1} = [\widetilde{\mathbf{V}}^{\mathcal{H}}\mathbf{R}_{\text{T},K_{22}}^{-1}\widetilde{\mathbf{V}}]_{1,1} = ([\widetilde{\mathbf{V}}]_{\bullet,1})^{\mathcal{H}}\mathbf{R}_{\text{T},K_{22}}^{-1}[\widetilde{\mathbf{V}}]_{\bullet,1} \\ &= \frac{\widetilde{\mathbf{b}}^{\mathcal{H}}\mathbf{R}_{\text{T},K_{22}}^{-1}\widetilde{\mathbf{b}}}{\|\widetilde{\mathbf{b}}\|^2}. \end{aligned} \tag{79}$$

B. Proof of Lemma 1

Based on (41) and (44), we can regard $[\mathbf{G}_2]_{\bullet,1} \doteq N_{\text{R}} \times 1$, as a vector of independent complex-valued Gaussians with variance of $1/2$ for the real and imaginary parts, and means

$$\mathbb{E}\{[\mathbf{G}_2]_{1,1}\} = \sqrt{x_2} = \|\widetilde{\mathbf{b}}\|[\mathbf{A}^{-\mathcal{H}}]_{1,1}, \quad \mathbb{E}\{[\mathbf{G}_2]_{i,1}\} = 0,\ i = 2 : N_{\text{R}}. \tag{80}$$

Thus, we have:

$$\frac{|[\mathbf{G}_2]_{1,1}|^2}{1/2} \sim \chi_2^2\left(\frac{x_2}{1/2}\right), \tag{81}$$

$$\frac{|[\mathbf{G}_2]_{i,1}|^2}{1/2} \sim \chi_2^2,\ i = 2 : N_{\text{R}} \Rightarrow \frac{|[\mathbf{G}_2]_{2,1}|^2}{1/2} + \cdots + \frac{|[\mathbf{G}_2]_{N_{\text{R}},1}|^2}{1/2} \sim \chi_{2(N_{\text{R}}-1)}^2. \tag{82}$$

Now, because $\mathbf{T}_2$ in (46) is upper triangular, we can write the first column of $\mathbf{G}_2 = \mathbf{U}_2\mathbf{T}_2$ as $[\mathbf{G}_2]_{\bullet,1} = [\mathbf{U}_2]_{\bullet,1}[\mathbf{T}_2]_{11}$, and then we may set

$$[\mathbf{U}_2]_{\bullet,1} = \frac{[\mathbf{G}_2]_{\bullet,1}}{\|[\mathbf{G}_2]_{\bullet,1}\|}, \quad [\mathbf{T}_2]_{1,1} = \|[\mathbf{G}_2]_{\bullet,1}\|. \tag{83}$$

Thus, we have

$$|[\mathbf{U}_2]_{1,1}|^2 = \frac{|[\mathbf{G}_2]_{1,1}|^2}{|[\mathbf{G}_2]_{1,1}|^2 + |[\mathbf{G}_2]_{2,1}|^2 + \cdots + |[\mathbf{G}_2]_{N_\mathrm{R},1}|^2} \overset{(81),(82)}{\sim} \frac{\chi_2^2\,(2x_2)}{\chi_2^2\,(2x_2) + \chi^2_{2(N_\mathrm{R}-1)}}, \tag{84}$$

which, based on [37], yields

$$|[\mathbf{U}_2]_{1,1}|^2 \;\sim\; Beta(1, N_\mathrm{R}-1, 2x_2), \tag{85}$$

$$\text{so that } \beta_1 \overset{(48)}{=} 1 - |[\mathbf{U}_2]_{1,1}|^2 \;\sim\; Beta(N_\mathrm{R}-1, 1, 2x_2). \tag{86}$$

The p.d.f. of β_1 is then given by [37]

$$f_{\beta_1}(v) = \sum_{n_2=0}^{\infty} \frac{e^{-x_2} x_2^{n_2}}{n_2!} \underbrace{\left(\frac{v^{(N_\mathrm{R}-1)-1}(1-v)^{(n_2+1)-1}}{\int_0^1 t^{(N_\mathrm{R}-1)-1}(1-t)^{(n_2+1)-1}\,\mathrm{d}t} \right)}_{=f_{\beta_3}(v;N_\mathrm{R}-1,n_2+1)}, \tag{87}$$

where $f_{\beta_3}(v; N_\mathrm{R}-1, n_2+1)$ is the p.d.f. of some variable $\beta_3 \sim Beta(N_\mathrm{R}-1, n_2+1)$. Thus, the n_1th moment of β_1 can be written from (87) as:

$$\mathbb{E}\{\beta_1^{n_1}\} = \sum_{n_2=0}^{\infty} \frac{e^{-x_2} x_2^{n_2}}{n_2!} \mathbb{E}\{\beta_3^{n_1}\} = \sum_{n_2=0}^{\infty} \frac{e^{-x_2} x_2^{n_2}}{n_2!} \frac{(N_\mathrm{R}-1)_{n_1}}{(n_2+N_\mathrm{R})_{n_1}}. \tag{88}$$

C. Proof of Lemma 2

First, let us expand $N_\mathrm{R} \times N_\mathrm{I}$ matrix $\mathbf{G}_2 \sim \mathcal{CN}(\mathbf{G}_{\mathrm{d},2}, \mathbf{I}_{N_\mathrm{R}} \otimes \mathbf{I}_{N_\mathrm{I}})$ from (41) — whose sole nonzero-mean column is $[\mathbf{G}_2]_{\bullet,1}$ — into an $N_\mathrm{R} \times N_\mathrm{R}$ matrix $\widehat{\mathbf{G}}_2 \sim \mathcal{CN}\left(\widehat{\mathbf{G}}_{\mathrm{d},2}, \mathbf{I}_{N_\mathrm{R}} \otimes \mathbf{I}_{N_\mathrm{R}}\right)$, by attaching an $N_\mathrm{R} \times N$ matrix $\widetilde{\mathbf{G}}_2$ with uncorrelated elements distributed as $[\widetilde{\mathbf{G}}_2]_{i,j} \sim \mathcal{CN}(0,1)$.

Then, paralleling (46), let us consider the QR decomposition of $\widehat{\mathbf{G}}_2$, i.e.,

$$\widehat{\mathbf{G}}_2 = (\mathbf{G}_2 \quad \widetilde{\mathbf{G}}_2) = \widehat{\mathbf{U}}_2 \widehat{\mathbf{T}}_2, \tag{89}$$

with $\widehat{\mathbf{U}}_2 \doteq N_\mathrm{R} \times N_\mathrm{R}$ unitary, i.e., $\widehat{\mathbf{U}}_2^{\mathcal{H}} \widehat{\mathbf{U}}_2 = \widehat{\mathbf{U}}_2 \widehat{\mathbf{U}}_2^{\mathcal{H}} = \mathbf{I}_{N_\mathrm{R}}$, and $\widehat{\mathbf{T}}_2 \doteq N_\mathrm{R} \times N_\mathrm{R}$ upper triangular with positive diagonal elements. By partitioning in (89) and using (46), we can write

$$\widehat{\mathbf{G}}_2 = (\mathbf{G}_2 \quad \widetilde{\mathbf{G}}_2) = (\mathbf{U}_2 \quad \widetilde{\mathbf{U}}_2) \begin{pmatrix} \mathbf{T}_2 & \widetilde{\mathbf{T}}_{12} \\ \mathbf{0} & \widetilde{\mathbf{T}}_{22} \end{pmatrix} = (\mathbf{U}_2 \mathbf{T}_2 \quad \mathbf{U}_2 \widetilde{\mathbf{T}}_{12} + \widetilde{\mathbf{U}}_2 \widetilde{\mathbf{T}}_{22}), \tag{90}$$

where $\widetilde{\mathbf{U}}_2 \doteq N_\mathrm{R} \times N$ satisfies $\widetilde{\mathbf{U}}_2^{\mathcal{H}} \widetilde{\mathbf{U}}_2 = \mathbf{I}_N$, $\widetilde{\mathbf{T}}_{12} \doteq N_\mathrm{I} \times N$, and $\widetilde{\mathbf{T}}_{22} \doteq N \times N$ is upper triangular with positive diagonal elements.

Now, given $[\mathbf{G}_2]_{\bullet,1}$ — i.e., given $[\mathbf{U}_2]_{\bullet,1}$ set as in (83) — the distribution of

$$\widehat{\mathbf{G}}_2 \overset{(89)}{=} \widehat{\mathbf{U}}_2 \widehat{\mathbf{T}}_2 = (\mathbf{U}_2 \quad \widetilde{\mathbf{U}}_2) \widehat{\mathbf{T}}_2 = ([\mathbf{U}_2]_{\bullet,1} \quad [\mathbf{U}_2]_{\bullet,2} \quad \ldots \quad [\mathbf{U}_2]_{\bullet,N_\mathrm{I}} \quad \widetilde{\mathbf{U}}_2) \widehat{\mathbf{T}}_2 \tag{91}$$

is invariant to unitary transformations of the columns $[\mathbf{U}_2]_{\bullet,i}$, $\forall i = 2 : N_\mathrm{I}$, and the columns of $\widetilde{\mathbf{U}}_2$. Thus, we may rewrite

$$\widehat{\mathbf{U}}_2 = (\mathbf{U}_2 \quad \widetilde{\mathbf{U}}_2) = \big([\mathbf{U}_2]_{\bullet,1} \quad (\mathbf{u}_2^0 \;\; \ldots \;\; \mathbf{u}_{N_\mathrm{I}}^0 \;\; \mathbf{u}_{N_\mathrm{I}+1}^0 \;\; \ldots \;\; \mathbf{u}_{N_\mathrm{R}}^0)\mathbf{P}\big), \tag{92}$$

where fixed orthonormal vectors $\mathbf{u}_2^0, \ldots, \mathbf{u}_{N_\mathrm{R}}^0$ are selected to form a basis with $[\mathbf{U}_2]_{\bullet,1}$, and $\mathbf{P} \doteq (N_\mathrm{R} - 1)\times(N_\mathrm{R} - 1)$ is unitary, Haar-distributed [18, Sec. III.E], not dependent on $[\mathbf{U}_2]_{\bullet,1}$.

Using the first row of $\mathbf{U}^0 = (\mathbf{u}_2^0 \;\; \ldots \;\; \mathbf{u}_{N_\mathrm{R}}^0) \doteq N_\mathrm{R} \times (N_\mathrm{R} - 1)$ from (92) to define the vector

$$\mathbf{q}^\mathcal{T} = [\mathbf{U}^0]_{1,\bullet}\,\mathbf{P} \doteq 1 \times (N_\mathrm{R} - 1), \tag{93}$$

the first row of $\widehat{\mathbf{U}}_2$ from (92) can be written as

$$[\widehat{\mathbf{U}}_2]_{1,\bullet} = ([\mathbf{U}_2]_{1,1} \quad \mathbf{q}^\mathcal{T}). \tag{94}$$

Then, based on $\widehat{\mathbf{U}}_2\widehat{\mathbf{U}}_2^\mathcal{H} = \mathbf{I}_{N_\mathrm{R}}$ and (94), we can write

$$1 = \|[\widehat{\mathbf{U}}_2]_{1,\bullet}\|^2 = |[\mathbf{U}_2]_{1,1}|^2 + \|\mathbf{q}\|^2 \Rightarrow \|\mathbf{q}\|^2 = 1 - |[\mathbf{U}_2]_{1,1}|^2. \tag{95}$$

Further, note from (93) that the vector

$$\frac{\mathbf{q}}{\|\mathbf{q}\|} = \frac{\mathbf{q}}{\sqrt{1 - |[\mathbf{U}_2]_{1,1}|^2}} \tag{96}$$

is uniformly distributed on the unit sphere $\mathbb{S}^{N_\mathrm{R}-2}$.

Finally, based on (92) and (94), we can write

$$[\widehat{\mathbf{U}}_2]_{1,\bullet} = ([\mathbf{U}_2]_{1,1} \quad [\mathbf{U}_2]_{1,2} \quad \ldots \quad [\mathbf{U}_2]_{1,N_\mathrm{I}} \quad [\widetilde{\mathbf{U}}_2]_{1,\bullet}) = ([\mathbf{U}_2]_{1,1} \quad q_1 \quad \ldots \quad q_{N_\mathrm{I}-1} \quad q_{N_\mathrm{I}} \quad \ldots \quad q_{N_\mathrm{R}-1}),$$

i.e., $[\mathbf{U}_2]_{1,2}, \ldots, [\mathbf{U}_2]_{1,N_\mathrm{I}}$ are the first $N_\mathrm{I}-1$ elements of $\mathbf{q}$. Thus, we can write, by also using (95),

$$\frac{|[\mathbf{U}_2]_{1,2}|^2 + \cdots + |[\mathbf{U}_2]_{1,N_\mathrm{I}}|^2}{1 - |[\mathbf{U}_2]_{1,1}|^2} = \frac{|q_1|^2 + \cdots + |q_{N_\mathrm{I}-1}|^2}{(|q_1|^2 + \cdots + |q_{N_\mathrm{I}-1}|^2) + (|q_{N_\mathrm{I}}|^2 + \cdots + |q_{N_\mathrm{R}-1}|^2)} = \beta_4,$$

which implies that, conditioned on $[\mathbf{G}_2]_{\bullet,1}$, i.e., on $[\mathbf{U}_2]_{\bullet,1}$, we have [37]

$$\beta_4 \;\sim\; Beta(N_\mathrm{I} - 1, N_\mathrm{R} - N_\mathrm{I}) = Beta(N_\mathrm{T} - 2, N), \tag{97}$$

$$\text{so that } \beta_2 = 1 - \beta_4 \;\sim\; Beta(N_\mathrm{R} - N_\mathrm{I}, N_\mathrm{I} - 1) = Beta(N, N_\mathrm{T} - 2), \tag{98}$$

which does not depend on $[\mathbf{U}_2]_{\bullet,1}$, i.e., our β_2 is independent of $\beta_1 \overset{(48)}{=} 1 - |[\mathbf{U}_2]_{1,1}|^2$.

D. Proof of Theorem 2

From the m.g.f. of the conditioned SNR in (49), based on the independence of β_2 and $\big(1 - |[\mathbf{U}_2]_{1,1}|^2\big)$, we have deduced (53) as follows:

$$\begin{aligned}
M_{\gamma_1}(s; x_1, x_2) &= \mathbb{E}_{(\beta_1,\beta_2)}\Big\{M_{\gamma_1}(s \mid \beta_1, \beta_2)\Big\} \overset{(49)}{=} \frac{1}{(1-\Gamma_1 s)^N}\mathbb{E}_{(\beta_1,\beta_2)}\Big\{\exp\{f_1(s)\beta_1\beta_2\}\Big\} \\
&= \frac{1}{(1-\Gamma_1 s)^N}\mathbb{E}_{\beta_1}\Big\{\mathbb{E}_{\beta_2}\Big\{e^{f_1(s)\beta_1\beta_2}\Big\}\Big\} = \frac{1}{(1-\Gamma_1 s)^N}\mathbb{E}_{\beta_1}\Big\{M_{\beta_2}\big(f_1(s)\beta_1\big)\Big\} \\
&\overset{(52)}{=} \frac{1}{(1-\Gamma_1 s)^N}\mathbb{E}_{\beta_1}\Big\{{}_1F_1\big(N; N_\mathrm{R}-1; f_1(s)\beta_1\big)\Big\} \\
&\overset{(56)}{=} \frac{1}{(1-\Gamma_1 s)^N}\sum_{n_1=0}^{\infty}\frac{(N)_{n_1}}{(N_\mathrm{R}-1)_{n_1}}\frac{f_1(s)^{n_1}}{n_1!}\mathbb{E}_{[\mathbf{U}_2]_{1,1}}\Big\{\beta_1^{n_1}\Big\} \\
&\overset{(88)}{=} \frac{1}{(1-\Gamma_1 s)^N}\sum_{n_1=0}^{\infty}\frac{(N)_{n_1}}{\cancel{(N_\mathrm{R}-1)_{n_1}}}\frac{f_1(s)^{n_1}}{n_1!}\sum_{n_2=0}^{\infty}\frac{e^{-x_2}x_2^{n_2}}{n_2!}\frac{\cancel{(N_\mathrm{R}-1)_{n_1}}}{(n_2+N_\mathrm{R})_{n_1}} \\
&\overset{(56)}{=} \frac{e^{-x_2}}{(1-\Gamma_1 s)^N}\sum_{n_2=0}^{\infty}\frac{x_2^{n_2}}{n_2!}{}_1F_1(N; n_2+N_\mathrm{R}; f_1(s)).
\end{aligned}$$

E. Derivation of the Expressions for x_1 and x_2

From Remark 1, the normalized vector $\mathbf{b}_\mathrm{n} = \frac{\mathbf{b}}{\|\mathbf{b}\|} \doteq N_\mathrm{T} \times 1$ does not depend on K. Using

$$\widetilde{\mathbf{R}} = \begin{pmatrix} 0 & \mathbf{0} \\ \mathbf{0} & \mathbf{R}^{-1}_{\mathrm{T},K_{22}} \end{pmatrix} \doteq N_\mathrm{T} \times N_\mathrm{T}, \tag{99}$$

$$\widetilde{\mathbf{r}}_{2,1} = (1 \quad -\mathbf{r}_{2,1}^{\mathcal{T}})^{\mathcal{T}} \doteq N_\mathrm{T} \times 1, \tag{100}$$

we can write μ_1 from (30) and $\widetilde{\mathbf{b}}^{\mathcal{H}}\mathbf{R}^{-1}_{\mathrm{T},K_{22}}\widetilde{\mathbf{b}}$ from (43) as follows:

$$\mu_1 = b_1^* - \widetilde{\mathbf{b}}^{\mathcal{H}}\mathbf{r}_{2,1} = \mathbf{b}^{\mathcal{H}}\widetilde{\mathbf{r}}_{2,1} = \|\mathbf{b}\|\,\mathbf{b}_\mathrm{n}^{\mathcal{H}}\widetilde{\mathbf{r}}_{2,1}, \tag{101}$$

$$\widetilde{\mathbf{b}}^{\mathcal{H}}\mathbf{R}^{-1}_{\mathrm{T},K_{22}}\widetilde{\mathbf{b}} = \mathbf{b}^{\mathcal{H}}\widetilde{\mathbf{R}}\mathbf{b} = \|\mathbf{b}\|^2\,\mathbf{b}_\mathrm{n}^{\mathcal{H}}\widetilde{\mathbf{R}}\mathbf{b}_\mathrm{n}. \tag{102}$$

Now, from (10), we have that $\|\mathbf{b}\|^2 = KN_\mathrm{R}N_\mathrm{T}/(K+1)$. Further, based on (11), we deduce that: $\big[\mathbf{R}^{-1}_{\mathrm{T},K}\big]_{1,1} \propto (K+1)$, and $\mathbf{R}^{-1}_{\mathrm{T},K_{22}} \propto (K+1)$, so that $\widetilde{\mathbf{R}} \propto (K+1)$; also, $\widetilde{\mathbf{r}}_{2,1}$ does not depend on K because $\mathbf{r}_{2,1}$ defined in (25) does not depend on K. These yield:

$$x_1 \overset{(32)}{=} \big[\mathbf{R}^{-1}_{\mathrm{T},K}\big]_{1,1}|\mu_1|^2 = \|\mathbf{b}\|^2\,\big[\mathbf{R}^{-1}_{\mathrm{T},K}\big]_{1,1}|\mathbf{b}_\mathrm{n}^{\mathcal{H}}\widetilde{\mathbf{r}}_{2,1}|^2 \propto KN_\mathrm{R}N_\mathrm{T}, \tag{103}$$

$$x_2 \overset{(43)}{=} \widetilde{\mathbf{b}}^{\mathcal{H}}\mathbf{R}^{-1}_{\mathrm{T},K_{22}}\widetilde{\mathbf{b}} = \|\mathbf{b}\|^2\,\mathbf{b}_\mathrm{n}^{\mathcal{H}}\widetilde{\mathbf{R}}\mathbf{b}_\mathrm{n} \propto KN_\mathrm{R}N_\mathrm{T}. \tag{104}$$

REFERENCES

[1] D. Tse and P. Viswanath, *Fundamentals of Wireless Communication*. Cambridge, UK: Cambridge University Press, 2005.

[2] D. Gesbert, M. Kountouris, R. Heath, C.-B. Chae, and T. Salzer, "Shifting the MIMO paradigm," *IEEE Signal Processing Magazine*, vol. 24, no. 5, pp. 36–46, Sep. 2007.

[3] H. Q. Ngo, M. Matthaiou, T. Duong, and E. Larsson, "Uplink performance analysis of multicell MU-SIMO systems with ZF receivers," *IEEE Transactions on Vehicular Technology*, vol. 62, no. 9, pp. 4471–4483, Nov 2013.

[4] F. Rusek, D. Persson, B. K. Lau, E. G. Larsson, T. L. Marzetta, O. Edfors, and F. Tufvesson, "Scaling up MIMO: Opportunities and challenges with very large arrays," *IEEE Signal Processing Magazine*, vol. 30, no. 1, pp. 40–60, 2013.

[5] J. Hoydis, S. ten Brink, and M. Debbah, "Massive MIMO in the UL/DL of cellular networks: How many antennas do we need?" *IEEE Journal on Selected Areas in Communications*, vol. 31, no. 2, pp. 160–171, 2013.

[6] L. Lu, G. Li, A. Swindlehurst, A. Ashikhmin, and R. Zhang, "An overview of massive MIMO: Benefits and challenges," *IEEE Journal of Selected Topics in Signal Processing*, vol. 8, no. 5, pp. 742–758, Oct 2014.

[7] E. Björnson, E. G. Larsson, and T. L. Marzetta, "10 myths and one grand question," *IEEE Communications Magazine, submitted*, Mar 2015.

[8] J. H. Winters, J. Salz, and R. D. Gitlin, "The impact of antenna diversity on the capacity of wireless communication systems," *IEEE Transactions on Communications*, vol. 42, no. 234, pp. 1740–1751, 1994.

[9] D. A. Gore, R. W. Heath, and A. J. Paulraj, "Transmit selection in spatial multiplexing systems," *IEEE Communications Letters*, vol. 6, no. 11, pp. 491–493, 2002.

[10] M. Kiessling and J. Speidel, "Analytical performance of MIMO zero-forcing receivers in correlated Rayleigh fading environments," in *IEEE Workshop on Signal Processing Advances in Wireless Communications (SPAWC'03)*, June 2003, pp. 383–387.

[11] R. U. Nabar, H. Bolcskei, and A. J. Paulraj, "Diversity and outage performance in space-time block coded Ricean MIMO channels," *IEEE Transactions on Wireless Communications*, vol. 4, no. 5, pp. 2519–2532, Sep 2005.

[12] M. Kang and M.-S. Alouini, "Capacity of MIMO Rician channels," *IEEE Transactions on Wireless Communications*, vol. 5, no. 1, pp. 112–122, Jan 2006.

[13] S. Jin, X. Gao, and X. You, "On the ergodic capacity of rank-1 Ricean-fading MIMO channels," *IEEE Transactions on Information Theory*, vol. 53, no. 2, pp. 502–517, Feb. 2007.

[14] M. McKay, A. Zanella, I. Collings, and M. Chiani, "Error probability and SINR analysis of optimum combining in Rician fading," *IEEE Transactions on Communications*, vol. 57, no. 3, pp. 676–687, Mar 2009.

[15] M. Matthaiou, C. Zhong, and T. Ratnarajah, "Novel generic bounds on the sum rate of MIMO ZF receivers," *IEEE Transactions on Signal Processing*, vol. 59, no. 9, pp. 4341–4353, Sep 2011.

[16] J. Li, M. Matthaiou, S. Jin, and T. Svensson, "Energy efficiency analysis of rank-1 Ricean fading MIMO channels," in *IEEE International Workshop on Signal Processing Advances in Wireless Communications (SPAWC'14)*, 2014, pp. 349–353.

[17] Q. Zhang, S. Jin, K.-K. Wong, H. Zhu, and M. Matthaiou, "Power scaling of uplink massive MIMO systems with arbitrary-rank channel means," *IEEE Journal of Selected Topics in Signal Processing*, vol. 8, no. 5, pp. 966–981, Oct 2014.

[18] C. Siriteanu, S. D. Blostein, A. Takemura, H. Shin, S. Yousefi, and S. Kuriki, "Exact MIMO zero-forcing detection analysis for transmit-correlated Rician fading," *IEEE Transactions on Wireless Communications*, vol. 13, no. 3, pp. 1514–1527, Mar 2014.

[19] C. Siriteanu, A. Takemura, S. D. Blostein, S. Kuriki, and H. Shin, "Convergence analysis of performance-measure

expressions for MIMO ZF under Rician fading," in *Australian Communications Theory Workshop, (AUSCTW'14), Sydney, Australia*, Feb. 2014.

[20] C. Siriteanu, A. Takemura, S. Kuriki, H. Shin, and C. Koutschan, "MIMO zero-forcing performance evaluation using the holonomic gradient method," *IEEE Transactions on Wireless Communications*, vol. 14, no. 4, pp. 2322–2335, Apr 2015.

[21] C. Siriteanu, A. Takemura, S. Kuriki, D. Richards, and H. Shin, "Schur complement based analysis of MIMO zero-forcing for Rician fading," *IEEE Transactions on Wireless Communications*, vol. 14, no. 4, pp. 1757–1771, Apr 2015.

[22] P. Kyosti, J. Meinila, L. Hentila, and *et al.*, "WINNER II Channel Models. Part I," CEC, Tech. Rep. IST-4-027756, 2008.

[23] C. Siriteanu, "Maximal-ratio eigen-combining for smarter antenna array wireless communication receivers," Ph.D. dissertation, Queen's University, Kingston, Canada, 2006. [Online]. Available: http://post.queensu.ca/~sdb2/PAPERS/thesis_siriteanu.pdf

[24] C. Siriteanu, Y. Miyanaga, S. D. Blostein, S. Kuriki, and X. Shi, "MIMO zero-forcing detection analysis for correlated and estimated Rician fading," *IEEE Transactions on Vehicular Technology*, vol. 61, no. 7, pp. 3087–3099, Sep 2012.

[25] E. Torkildson, U. Madhow, and M. Rodwell, "Indoor millimeter wave MIMO: Feasibility and performance," *IEEE Transactions on Wireless Communications*, vol. 10, no. 12, pp. 4150–4160, Dec 2011.

[26] G. A. Ropokis, A. A. Rontogiannis, P. T. Mathiopoulos, and K. Berberidis, "An exact performance analysis of MRC/OSTBC over generalized fading channels," *IEEE Transactions on Communications*, vol. 58, no. 9, pp. 2486–2492, 2010.

[27] C. Koutschan, "Advanced applications of the holonomic systems approach," Ph.D. dissertation, Research Institute for Symbolic Computation (RISC), Johannes Kepler University, Linz, Austria, 2009. [Online]. Available: http://www.risc.jku.at/research/combinat/software/HolonomicFunctions/

[28] ——, "HolonomicFunctions (user's guide)," RISC Report Series, Johannes Kepler University, Linz, Austria, Tech. Rep. 10-01, 2010. [Online]. Available: http://www.risc.jku.at/research/combinat/software/HolonomicFunctions/

[29] B. Buchberger, "Bruno Buchberger's PhD thesis 1965: An algorithm for finding the basis elements of the residue class ring of a zero dimensional polynomial ideal," *Journal of Symbolic Computation*, vol. 41, no. 34, pp. 475 – 511, 2006. [Online]. Available: http://www.sciencedirect.com/science/article/pii/S0747717105001483

[30] Z. Lin, L. Xu, and N. K. Bose, "A tutorial on Gröbner bases with applications in signals and systems," *IEEE Transactions on Circuits and Systems I: Regular Papers*, vol. 55, no. 1, pp. 445–461, 2008.

[31] Q. Geng, S. Kannan, and P. Viswanath, "Interactive interference alignment," *IEEE Journal on Selected Areas in Communications*, vol. 32, no. 9, pp. 1699–1706, 2014.

[32] M. Fozunbal, S. W. McLaughlin, R. W. Schafer, and J. M. Landsberg, "On space-time coding in the presence of spatio-temporal correlation," *EEE Transactions on Information Theory*, vol. 50, no. 9, pp. 1910–1926, 2004.

[33] C. Koutschan. `Mathematica` notebook `Rank1Rice.nb` with derivations of differential equations using the `HolonomicFunctions` package. [Online]. Available: http://www.koutschan.de/data/rank1rice/

[34] J. E. Gentle, *Matrix algebra: theory, computations, and applications in statistics*. Springer, 2007.

[35] F. W. J. Olver, D. W. Lozier, R. F. Boisvert, and C. W. Clarck, Eds., *NIST Handbook of Mathematical Functions*. Cambridge University Press, 2010. [Online]. Available: http://dlmf.nist.gov/

[36] K. E. Muller, "Computing the confluent hypergeometric function, $M(a, b, x)$," *Numerische Mathematik*, vol. 90, no. 1, pp. 179–196, 2001.

[37] R. Chattamvelli, "A note on the noncentral beta distribution function," *American Statistician*, vol. 49, no. 2, pp. 231–234, 1995.